Mapping of seafloor hydrothermally altered rocks using geophysical methods: Marsili and Palinuro seamounts, southern Tyrrhenian Sea

Marco Ligi[1]*, Luca Cocchi[2], Giovanni Bortoluzzi[1], Filippo D'Oriano[1], Filippo Muccini[2], Fabio Caratori Tontini[3], Cornel E. J. de Ronde[3], Cosmo Carmisciano[2]

[1] *Istituto di Scienze Marine, CNR, Via Gobetti 101, 40129, Bologna, Italy*

[2] *Istituto Nazionale di Geofisica e Vulcanologia, Roma2, Via Pezzino Basso 2, 19025, Fezzano (La Spezia), Italy.*

[3] *GNS Science, Ocean Exploration Section, 1 Fairway Dr, Avalon, Lower Hutt 5040, New Zealand.*

* To whom correspondence should be addressed. E-mail: marco.ligi@bo.ismar.cnr.it

Abstract

Hydrothermal alteration processes involve mineralogical, chemical and textural changes as a result of hot aqueous fluid-rock interaction under evolving boundary conditions. These changes affect the physico-chemical properties of the rocks, enabling high-resolution geophysical prospecting to be an important tool in the detection of seafloor hydrothermal alteration. Here we present the results of recent geophysical investigations of Marsili and Palinuro volcanic complexes, southern Tyrrhenian Sea during the 2010 TIR10 and 2011 MAVA2011 cruises by the *R/V Urania*. The new dataset includes a dense grid of multibeam bathymetry; seafloor reflectivity, magnetic and gravity lines; and high-resolution single (CHIRP) and multichannel seismic profiles. The surveys were focused on areas known to host intense hydrothermal alteration in order to provide a more detailed description of the Marsili and Palinuro hydrothermal systems. Ground-truthing was based on earlier discoveries of hydrothermal vents and their associated deposits, and on direct observations made by ROV dives. High-resolution morpho-bathymetry, sonar reflectivity, rock magnetization and density distribution together enabled us to assess the extent of seafloor hydrothermal alteration and its relationship to local volcanic and tectonic structures. Hydrothermal alteration associated with the Marsili seamount is largely distributed along primary volcano-tectonic structures at the ridge crest. By contrast, at Palinuro hydrothermal alteration is mostly associated with secondary volcanic structures such as collapsed calderas and volcanism reactivation along ring-faults. In particular, evidence for intense hydrothermal activity occurs at Palinuro where volcano-tectonic features interact with regional tectonic structures.

Introduction

Hydrothermal systems and their corresponding alteration patterns at convergent plate boundaries are considered to be a better modern analogue of processes responsible for volcanogenic massive sulfide ore deposits than hydrothermal systems located along mid-ocean ridges (Skinner, 1983; Ishibashi and Urabe, 1995; de Ronde et al., 2003a, 2003b). Remote sensing of potential fields such as gravity and magnetics is important in evaluating the extent of seafloor hydrothermal alteration because they can aid in the location of potential mineral deposits, rather than relying solely on locating active vent sites on the seafloor. Thus, potential field methods and remote sensing of submarine arc volcanoes will enhance our understanding of the formation of hydrothermal seafloor massive sulfide deposits (Hannington et al., 1995; de Ronde et al., 2011).

Hydrothermal solutions or fluids produce physico-chemical changes in the rocks through which they circulate via chemical reactions, resulting in the formation of new mineral assemblages that tend to approach equilibrium thorough processes of dissolution and precipitation (e.g., Pirajno, 2010). These changes, affecting porosity, density and magnetization of the rocks, enable high-resolution geophysical prospecting to determine the areal distribution of submarine hydrothermal alteration (Woodward and Mumme, 1993; Tivey and Dyment, 2010; Caratori Tontini et al., 2010; Caratori Tontini et al., 2012a,b). Measurements of gravity and magnetics, in particular, can provide insight into submarine hydrothermal system formation as hydrothermal processes can reduce rock densities and can also decrease, and even nullify the magnetic signature of the volcanic host rocks (Tivey and Dyment, 2010; Caratori Tontini et al., 2012a,b). Ship-borne geophysical investigations provide the spatial resolution required to map and model shallow water (< 500 m) hydrothermal vent fields. By contrast, near-bottom

geophysical data, typically obtained using AUVs (autonomous underwater vehicles), are required for deep-water systems (e.g., Caratori Tontini et al., 2012a).

Submarine volcanic structures affected by hydrothermal circulation may show anomalous variations in the corresponding gravity field as a result of density changes due to enhanced local permeability, and by alteration of the rock (Caratori Tontini et al., 2010). In addition, density variations can also be due to solidification of a relatively deep magmatic body that releases latent heat of fusion during cooling, which is ultimately responsible for hydrothermal convection at the site (Wallace, 2005), these magmatic bodies can be detected by gravity data inversion. Moreover, faults and fractures imaged by seismic reflection surveys can provide additional constraints on seafloor alteration patterns considering their orientation and distribution commonly control pathways of hydrothermal fluid upflow (e.g., Embley et al., 2012). A clearer picture of shallow seafloor hydrothermal manifestations can also be achieved by bathymetric and sonar backscatter imaging of the seafloor. Backscatter from side-scan and/or multibeam data collected over hydrothermal altered areas may be differentiated from those areas host to soft sediments, or relatively fresh volcanic rocks. That is, sites host to hydrothermal activity may have higher backscatter than seafloor covered by soft sediments because hydrothermal systems that form vents and sulfide deposits can increase seafloor roughness. By contrast, high levels of backscatter commonly attributed to fresh lavas forming hummocky terrains can be decreased as a consequence of hydrothermal alteration. In summary, high-resolution acoustic surveys can be used to determine which sectors of the volcano are affected by hydrothermal circulation, as given by the presence of extensive seafloor alteration and massive sulfide and/or chimney fields (e.g., Klauche et al., 2008; Ondreas et al. 2009).

We present here results from ship-borne geophysical surveys over Marsili and Palinuro volcanic complexes in the southern Tyrrhenian Sea. Ship-derived multibeam bathymetry, reflectivity (backscatter), gravity, magnetics, and single and multichannel seismic reflection data were acquired during the 2010 TIR10 and 2011 MAVA11 expeditions with the R/V *Urania*, in a study of seafloor hydrothermal activity along the Aeolian Arc. Complimentary, deep-tow magnetic data collected during MAVA11 are presented and discussed in a companion paper by Caratori Tontini et al. (2013, this issue). Our work focuses on volcano-scale geophysical signature attributed to hydrothermal processes occurring at Marsili and Palinuro in order to estimate the regional extent of hydrothermal alteration and its relationship to local volcanic and tectonic structures.

Geological setting

The tectonic setting of the central Mediterranean Sea results from African and Eurasian plate convergence and collision. Evolution of the Mediterranean area has been driven since Oligocene times by the sinking and the eastward retreat of the Ionian-African slab, with the consequent eastward migration of the Alpine/Apennine collisional belt (Malinverno and Ryan, 1986; Kastens et al., 1988; Doglioni 1991, 1999, 2004). The eastward retreat of the subduction system is associated with stretching of the continental crust and basin formation that occurred progressively in the Provencal and Valencia areas. Since Tortonian times (i.e., 11.6 to 7.2 Ma), the rollback process imposed E-W and NW-SE extension forming the Vavilov and Marsili back arc basins (Royden 1988; Patacca et al., 1990; Faccenna et al., 1997). Crustal thinning and oceanic crustal accretion, which occurred in the Vavilov Basin during the Late Miocene and Pliocene, migrated southeast-ward and formed the Marsili back-arc basin during the

Late Pliocene-Quaternary. Consequently, arc-related volcanism migrated in a southeast direction, from Sardinia to the current position of the Aeolian Arc, forming the present-day arc and back-arc configuration of the southern Tyrrhenian area (Fig. 1). Thus, the southern Tyrrhenian region is characterized by the transition from a nearly oceanic crustal domain (i.e., the Marsili Basin) to a continental margin offshore Sicily and Calabria, in a complex geodynamic framework (Doglioni, 1991; Patacca et al., 1990; Mantovani et al., 1996; Argnani 2009; Ventura et al., 2012).

The Aeolian Arc is located within regions with different stress regimes (De Astis et al., 2003). North-south compression occurs to the western part of this region, and NNW-SSE dextral strike-slip in the eastern part. The Aeolian Arc has an arcuate shape, open to the west, and includes volcanic islands as well as large submarine volcanoes (Fig. 1). Calc-alkaline and shoshonitic volcanism occurred in the area for the last 400 ,000 years, with the exception of the older edifices of Sisifo (1.3 Ma) and Filicudi (1 Ma) (Bortoluzzi et al., 2010 and reference therein). Today, active volcanism occurs on Lipari and Vulcano, located in the central part of the Aeolian Arc, and on Panarea and Stromboli, in its eastern part. Panarea and Stromboli are part of a 45 km long volcanic belt aligned in a NE direction, parallel to the regional fault system affecting the Calabrian margin. From late 2002 to mid-2003 a pronounced episode of degassing occurred on Panarea (Aliani et al., 2010), while significant eruptions occurred on Stromboli.

Evidence of hydrothermal processes occurring on the submarine parts of the Aeolian Arc has been documented with the presence of sulfide deposits on Palinuro and Marsili, and Fe-Mn hydroxides on other seamounts (Bonatti et al., 1972; Gamberi et al., 1997; Dekov and Savelli, 2004; Dekov et al., 2006, 2007, 2009). The first systematic

survey over the Aeolian submarine volcanoes for hydrothermal plumes was conducted during the Aeolian2007 cruise with the aim of locating seafloor hydrothermal vent fields (Sprovieri et al., 2008; Lupton et al., 2011). The volcanoes were surveyed using a CTDO (conductivity-temperature-depth-optical) rosette profiling system equipped with Niskin bottles that enabled discrete water samples to be collected. Evidence of active hydrothermal activity was found over several of the submarine volcanoes, including Palinuro and Marsili, from $^{3}He/^{4}He$ results (Lupton et al., 2011).

The Marsili basin is characterized by crustal thinning and the existence of an oceanic spreading segment (Marani and Trua, 2002). Here, the evolution of the backarc basin is related to an immature stage of the oceanic spreading centre (Nicolosi et al., 2006) that started around 2 Ma and continued until 0.3 Ma with continuous accretion, but with spreading rates decreasing from <60 mm yr^{-1} to <20 mm yr^{-1} over that time interval (Cocchi et al., 2009). The flat, deep seafloor of the central part of the basin is disrupted by the Marsili seamount. The emplacement and accretion of the seamount over the last 1 million years is interpreted as the result of a strong magmatic pulse, in combination with slow seafloor spreading rates (Cocchi et al., 2009). In this context, the Marsili seamount is considered to be a 'super-inflated' ridge (Marani and Trua, 2002), i.e., it is a ~55 km-long linear volcanic edifice striking N15°E, that rises from a depth of ~3,500 m shoaling to ~500 m in its central-northern part (Fig. 2). Recent geophysical surveys are consistent with widespread hydrothermal activity occurring on the shallowest portion of the seamount (Caratori Tontini et al., 2010; Lupton et al., 2011). Combined gravity and magnetic data revealed an anomalous, poorly magnetized and low density mass up to 2 km deep within the volcanic edifice, interpreted by Caratori Tontini et al. (2010) to be a sub-seafloor hydrothermal system. Despite direct

observations at Marsili of hydrothermal features such as sulfide deposits and chimney fields (Petersen et al., 2008), a comprehensive model of the hydrothermal system and any understanding of the relationship between the shallow hydrothermal features and local volcano-tectonic setting has not been forthcoming.

The Palinuro volcanic complex is located ~30 km NE of Marsili seamount and rises from the abyssal plain to a depth of ~80 m in its central part (Fig. 1). It strikes for ~60 km from west to east with a basal width of ~25 km (Passaro et al., 2010). Eight separate volcanic cones that coalesce at their base, forming an E-W elongated edifice, characterise Palinuro. The morphology of this complex is far more intricate than the simple shapes of the strato-volcanoes that project above sealevel along the Aeolian Arc, such as Stromboli. The southernmost flank of Palinuro, which bounds the northeastern part of the Marsili basin, shows steep scarps down to a maximum depth of 3,400 m. The central part of the complex is built up by two shallow cones that shoal to water depths of ~80 and ~150 m, respectively (Fig. 1). K-Ar dating of fresh lavas sampled from the top of the shallower major cone give an age of ~350,000 years (Colantoni et al., 1981). Andesite rocks recovered from Palinuro show a clear affinity to calc-alkaline volcanism commonly associated with the Aeolian islands. However, it is still matter of debate whether or not the Palinuro is structurally part of the Aeolian Arc (e.g., Passaro et al., 2010).

The Palinuro volcanic complex is host to hydrothermal vent fields (Peters et al. 2011; Petersen et al., 2008) that are host to hydrothermal deposits rich in galena, pyrite and sphalerites that are partially covered by sediments (Colantoni et al., 1981; Minniti and Bonavia, 1984). These volcanogenic massive sulfides have been located only at a water depth of ~600 m in the western sector of the volcanic complex. However, the full

extent of hydrothermal alteration at Palinuro is still poorly defined, given that exploration of the seafloor here has been limited to a few specific areas.

Regional magnetic data covering the Palinuro volcanic complex show a clear difference in rock magnetization between the eastern and western parts of the complex (Caratori Tontini et al., 2009). That is, the eastern part is the least magnetized area of the entire volcanic complex, while the central and western parts show sharp variations in magnetic anomaly amplitude, decreasing to around 0 nT in places where hydrothermal deposits have been discovered (Colantoni et al., 1981; Minniti and Bonavia, 1984). Changes in Palinuro magnetic rock properties have been interpreted in terms of hydrothermal alteration of the host volcanic rock (Caratori Tontini et al., 2010).

Methods

The TIR10 and MAVA11 cruises were carried out with the R/V *Urania,* which is equipped with differential GPS and SEAPATH positioning systems. The vessel is also equipped with single and multibeam bathymetric systems and integrated geophysical and oceanographic data acquisition systems, including acoustic doppler current (ADCP) and sub-bottom profilers (CHIRP).

Bathymetric data were acquired during the cruises using an EM710 Kongsberg-Simrad multibeam system, operating at ~70 kHz with 400 beams, with a resolution of 1°x2° and a 150° aperture. A sound velocity probe, located 1 m above the sonar head on the ship's keel, continuously provided the surface water acoustic velocity data required for the beam-forming. Conductivity-temperature-depth (CTD) casts using a *SeaBird SBE 911* probe were used to determine sound velocities within the water column. The

multibeam data were processed by the Kongsberg Neptune/Poseidon packages; spatial analysis and mapping were performed using the GMT (Wessel and Smith, 1995) and PLOTMAP (Ligi and Bortoluzzi, 1989) packages. Digital terrain models and reflectivity images were produced down to a horizontal resolution of 2.5 m in the shallower parts (<200 m) of the Palinuro volcanic complex.

Ship-borne magnetic data were acquired using a *SeaSpy* marine magnetometer built by Marine Magnetics Inc. that was towed ~185 m astern of the vessel. The acquired data were recorded using *Marine Magnetics Sealink* software. Total-field magnetic data, after de-spiking, were corrected for diurnal variations using reference data from the l'Aquila observatory (INGV-InterMagnet). Magnetic anomalies were obtained by removing the international geomagnetic reference field (IGRF) and then reduced the data to the North Pole by phase shifting them using the regional inclination and declination values of the IGRF. The intensity of the rock magnetization has been obtained by inversion of the reduced-to-the-pole magnetic anomalies using a Fourier method that assumes a variable thickness of the magnetized layer, bounded at the top by the seafloor and at the bottom by a horizontal layer placed 2 km below the maximum depth of the seafloor in the area (Parker, 1973; Caratori Tontini et al., 2008).

Magnetic gradiometer data were acquired during the 2006 PROMETHEUS cruise with the R/V *Universitatis* (Paltrinieri et al., 2006). Two *G880 Cesium* marine magnetometers were used in a longitudinal configuration and placed 250 m apart, while the survey followed lines oriented 108° N, or perpendicular to the Marsili ridge axis. Diurnal variations and the regional magnetic field do not affect measured magnetic gradients, given the short distance separating the sensors. Thus, the horizontal gradient was computed by the difference between the two sensor measurements divided by their

distance. In order to reduce the effects on the data of the high relief of the Marsili ridge, low frequency signals were removed from the measured magnetic horizontal gradient, following the windowed method of Grauch and Johnston (2002), which helps to separate local, from regional gradients.

Gravity data were collected during the 2011 MAVA11 cruise using a *LaCoste & Romberg* air/sea model gravity meter controlled by an *UltraSys* system (provided by GNS Science). The instrument was located close to the centre of gravity of the ship and interfaced to the navigation system of the vessel for real-time data geo-referencing. Gravity values were recorded at 6 s intervals and smoothed with mean value every 60s corresponding to an average distance of ~150 m between data points registered during the geophysical profiling, as the ship travelled at speed of 5-6 knots. Gravity reference points were obtained at the beginning and the end of the expedition in order to estimate the mechanical drift of the gravimeter. In addition, the system was calibrated with an absolute gravity station located at the position "P2" of the Maritime Station berth of Naples. The normal gravity (Geodetic Reference System 1980), Eotvos and drift corrections have been applied to the data in order to obtain the free air gravity anomaly. The local density distribution was estimated by applying a Bouguer correction. The high relief of both the Marsili and Palinuro volcanic complexes also requires a topographic correction. Thus, the complete Bouguer correction was obtained by replacing the overlying water column (density of 1030 kg/m^3) with a layer of crustal material (density of 2670 kg/m^3). Magnetic and gravity data acquired during this study were then merged with those collected during previous expeditions in order to obtain a more detailed geophysical analysis of the region.

An *Edgetech 4200* (100 and 400 kHz) side-scan sonar was used during the deep

tow magnetic survey (MAVA11). The system was interfaced to a 3,000 m depth-rated *Seaspy* magnetometer tow-fish (Caratori Tontini et al., 2013, this issue).

Visual surveys were conducted along the crest of Marsili with R/V *Daedalus* on May 2011, using the remotely operated vehicle (ROV) *Pluto Palla* capable of working in water depths of up to 4,000 m.

Multichannel reflection seismic lines were acquired during the 2010 TIR10 cruise (Doglioni et al., 2012) as part of the Italian CROP Project (http://www.crop.cnr.it). The seismic source used was a tuned array of 3 SERCEL GI-GUN (2x45/45, 75/75 in^3), towed at 5 m depth, and a pressure of 140 bar. The data were acquired by a SERCEL digital streamer with 96 channels and a 12.5 m group-interval, towed at 4-7 m depth. The sampling rate was 0.5 ms with a record length of 12 s, SEG-D storage format on disk, while shot interval was set at 37.5 m distance travelled. The seismic data have been processed using an industrial package (Disco/Focus) by Paradigm Geophysical, following a standard procedure that produces time migrated sections. Additional steps were applied to: (a) remove bottom surface multiples using a 2D SRME (Surface-Related Multiple Elimination) technique and adaptive filters, (b) attenuate random and coherent noise by filtering in the common shot, offset and receiver domains, as well as f-k and tau-p domains, (c) iteratively refine the velocity model used for normal move out and migration; and (d) perform post-stack depth migration. Post stack depth migration was achieved by a finite difference approximation to the wave equation using a velocity model obtained from the time migration model and adjusted iteratively in order to minimize the over/under migration effects at depth.

Results

Marsili Seamount

The ridge crest of the Marsili volcanic complex trends SSW-NNE and is abruptly disrupted and offset ~1 km to the east at its shallowest part (~39°16.8’ N) where the most recent volcanic activity has been observed (see Figs 2 and 3). In this area, andesitic pillow and sheet lava flows have been dated to be ~100,000 years old (Trua et al., 2011). The sharp crest striking northwards around 39°15.5' N intersects a wide plateau that is populated by numerous small volcanic cones with diameters up to 200-300 m, forming segmented volcanic ridges. The largest ridge, 2.2 km long and 0.7 km wide, at 39°16.5' N includes two coalesced volcanic edifices with ~100 m-diameter summit craters, with a small 780 m deep depression located south of the crest. The summit of this ridge shoals to 490 m. It is bounded by steep scarps to the west and east and is cut by several normal faults along axis (Fig. 3). In general, the western scarp of the summit area of Marsili is marked by high reflectivity whereas a wide, low-reflectivity region characterises the NE sector (Fig. 2). The central area of Marsili shows a variable reflectivity pattern. High reflectivity characterises the flanks of the small volcanic ridges and cones. South of the plateau, high backscatter characterises both flanks of the Marsili ridge, with several low reflectivity areas along the S-N trending crest of the volcano (Fig. 2).

The plateau segmenting the ridge-like morphology of Marsili can be correlated with pronounced magnetic and gravity lows (Figs 2c and 2d), previously described by Cocchi et al. (2009) and Caratori-Tontini et al. (2010). This area is host to hydrothermal Fe-Mn-oxyhydroxides-rich chimneys, as observed during ROV dives. For example, images obtained from ROVs at the crest (summit) of the Marsili ridge show several extinct sulfide chimneys up to 3 m tall, at a depth of 495 m (see Figs 2, 3 and 4). Hydrothermal manifestations, including what appears to be low temperature venting

together with sulfide deposits, were also observed south of the plateau, at a depth of ~600 m (Fig. 4), coincident with several gravity minima along the ridge crest, as given in the newly compiled Bouguer anomaly map (see Fig. 2c).

Palinuro Seamount

The Palinuro volcanic complex consists of several volcanic edifices that are either overlapping and/or which have coalesced, and are interpreted as a sequence of structurally controlled volcanic cones and collapsed calderas that developed under a regional stress field (Fig. 5). A study of the seafloor morphology suggests that structural elements trending WNW-ESE, WSW-ENE and ~N-S have played a major role in the evolution of the volcanic complex, controlling the location and shape of the volcanic edifices. The major cones are elongated in a WNW-ESE direction and are located at intersections of WNW-ESE and WSW-ENE oriented fault systems; volcanic ridges and collapsed calderas are mainly controlled by a ~N-S striking fault system (Figs 1 and 5). Morphological and geological evidence suggests that the volcanic cones may be emplaced on a pre-existing boundary formed by WNW-ESE and WSW-ENE fault systems that separate the northern continental domain from the southern oceanic Marsili Basin (Figs. 1 and 5). Following Passaro et al. (2010) the Palinuro volcanic complex has been divided into western, central and eastern sectors, based on morphological and structural differences (see Fig. 5).

Western sector. This sector is characterised by two wide volcanic structures (Figs 5 and 6): 1) a 4 km-wide sub-circular flat depression dominates the westernmost area, with a WSW-ENE striking scarp shaping its southern flank (Fig. 5); and 2) clusters of small volcanic cones surrounding a ~8 km-wide depression, semi-elliptical shape and

elongated WNW-ESE dominates the easternmost area (Fig. 6a). The easternmost depressed area is bordered by an arcuate shaped, NE striking scarp to the west and a WNW-ESE trending volcanic ridge to the north (Fig. 6). This morphology suggests a caldera-forming gravitational collapse event of a pre-existing edifice has occurred, followed by reactivation of volcanic activity along ring faults, with the volcanic cones emplaced along the caldera rim. The linear scarp to the west could be the solitary remains of the original volcano flank. A strong magnetic anomaly minimum is present in the NE sector of the caldera (Fig. 7a). Bouguer anomaly lows are centered on the caldera rim with local minima seen in the SW sector and again over the NE volcanic ridge (Fig. 7b). High multibeam reflectivity marks the steepest scarps that bound the depression that is the bottom of the caldera (Fig. 6b). High reflectivity is also found along the crest of the NE volcanic ridge and in widespread, relatively low relief areas within the caldera, especially near its western margin. Regions outside the caldera show lower reflectivity.

Central sector. The two largest volcanic cones located in the central sector of the Palinuro volcanic complex have flat, circular summits, with diameters of ~0.8 and ~2.5 km, respectively (Figs 8 and 9). The volcanic edifices display several gullies and incisions, mostly arranged in a radial pattern around the summits (Fig. 8a). The flat, shallow tops of the two cones with depths of 82 m and 147 m, respectively, are interpreted as wave-cut marine terraces due to lower sealevel in the past. The flanks of the two cones show low reflectivity, with higher values associated with narrow ridges that project radially outwards from the cone flanks, corresponding to narrow intervening ridges between small gullies. The flat tops show concentric bands and patchy areas of high reflectivity corresponding to relict crater rims and isolated rocky outcrops,

respectively (Fig. 8b). In addition, a relatively wide, low relief area of high backscatter is observed in the NW sector of the largest cone (Fig. 8b). Circular shaped regions of low magnetic anomaly were seen to coincide with the two cone summits that negatively correlate with the bathymetry, indicating vanishing magnetization (Fig. 9a). Moreover, these same two cone summits correlate with relatively low Bouguer gravity anomalies (i.e., low density rocks; see Fig. 9b).

The multichannel seismic line TIR10/12 runs S-N, eastwards of the above-mentioned two volcanic cones; it crosses the lower eastern flank of a volcanic edifice, that has a summit crater 75 m deeper than the surrounding crater rim, at a depth of ~570 m (see Fig. 9). Further to the north, the seismic line intersects a major fault (F_1 in Figs. 5 and 11) that trends WNW-ESE. This fault separates the aforementioned volcanic edifice from the easternmost edifice of the central Palinuro volcanic complex, that shapes the south-western flank. Further north again, the seismic line cuts a sub-circular depression with a diameter of ~2 km that we believe is likely related to the caldera-forming gravitational collapse event. The seismic section shown in Figure 11 highlights the role played by ring faults in the caldera formation (e.g., F_1). For example a well stratified volcanic sequence in the north of the section, that dips to the north, is likely comprised of numerous volcaniclastic layers (which are less reflective; or the light-gray layers) interbedded with lava flows (which are more reflective; or the dark-gray layers), and which is then entirely collapsed and offset within the caldera (Fig. 11b). The northern border of the caldera is cut by a major regional, tectonic feature (F_2 in Figs 5 and 11) that strikes WSW-ENE that has previously been identified as a strike-slip fault (Passaro et al., 2010; 2011). Despite a smooth, almost-flat seafloor marking the bottom of the caldera, a relatively high backscatter is recorded in this area (Fig. 12).

Eastern sector. The easternmost sector of the Palinuro volcanic complex appears to be completely different from the others, where the volcanic features appear structurally controlled by a WNW-ESE trending faults and cut by mainly N-S trending structures (Fig. 5). High resolution geophysical investigations over the eastern sector are currently not available, although this sector appears to be the least magnetized area of the volcanic complex (Caratori Tontini et al., 2009).

Discussion

The ridge crest at Marsili and the westernmost sector of the Palinuro volcanic complex have been the subject of several studies focused on shallow submarine hydrothermal systems in a back-arc and arc setting (Minniti and Bonavia, 1984; Colantoni et al., 1981; Marani et al., 1999; Petersen et al., 2008; Monecke et al., 2009; Caratori Tontini et al., 2010). The magnetic anomaly of the Marsili ridge presented in this study confirms the main conclusion of Caratori Tontini et al. (2010), i.e., that the measured summit magnetic minimum is due to a decrease in rock magnetization related to hydrothermal alteration. The deep tow magnetic data show a similar magnetic pattern to the ship-derived data presented here. However, the region with low magnetization is narrower and mainly limited to the summit plateau area using the near-bottom data of Caratori Tontini et al. (2013, this issue).

In this study we have attempted to better identify the boundaries of areas affected by hydrothermal alteration by using magnetic gradiometer data, where the high frequency components are emphasized, thus providing information on magnetization of the shallow crust possibly influenced by hydrothermal circulation. The results show that the margins of the regions with decreasing rock magnetization occur in the north-central

sector of the Marsili ridge and extend the potential areas of hydrothermal alteration into the southern part of the ridge (Fig. 2d). This conclusion is supported by local areas of low magnetization south of the summit plateau seen in the deep tow data (Caratori Tontini et al., 2013, this issue). Gravity data from the summit area of the volcano show a density lower than that typical of basaltic and/or andesitic rocks (Caratori Tontini et al., 2010, Fig. 2c); the observed density variations have been modelled as hydrothermal alteration affecting the top of the edifice down to ~2 km below the seafloor, with sub-seafloor volcanic rocks characterized by high porosity (Caratori Tontini et al., 2010). These observations are supported by our new high-resolution gravity compilation of the summit region obtained by merging new MAVA11 data with those collected during earlier expeditions (Fig. 2c). In addition, our Bouguer anomaly map shows that several local gravity minima occur along the crest of the volcano, and are not limited to the north-central part of the seamount. We thus suggest a probable extension of the region affected by hydrothermal alteration towards the southern end of the Marsili volcanic ridge, consistent with ROV observations of seafloor hydrothermal activity (Fig. 4).

The westernmost sector of the Palinuro volcanic complex has a caldera-like structure. The bathymetry reveals a sub-circular rim related to the collapse of a volcanic edifice after cessation of volcanic activity (Marani and Gamberi, 2004). Post-collapse volcanic activity resulted in the growth of small cones along the caldera rim where we infer hydrothermal alteration to be localized. Parts of the volcanic structure host to hydrothermal activity are covered by fine-grained hemipelagic or pelagic sediments that contain disseminated sulfides, Mn–Fe oxides and clay minerals (Minniti and Bonavia, 1984; Tufar, 1991; Eckhardt et al., 1997; Marani et al., 1999, Monecke et al., 2009; Peters et al., 2011). Recent ROV surveys at Palinuro have focused on a vent field

located in a small topographic depression on top of the westernmost volcanic edifice of the northern volcanic ridge (Petersen et al., 2008; Monecke et al., 2009). Fine-grained sediments that locally are marked by patchy discolorations cover the seafloor in this area. Delicate chimney-like iron oxides structures festooned with bacterial mats indicate low-temperature hydrothermal activity (Monecke et al., 2009). Cores of the sub-seafloor portion of the active fluid venting area, recovered at closely spaced stations using the shallow drilling system Rockdrill of the British Geological Survey, show up to 5 m-thick deposits of continuous massive sulfides and sulfates. Massive sulfides were encountered at depths from a few centimeters up to several meters below a thick cover of unconsolidated sediments (Petersen and Monecke, 2009, Petersen et al., 2013, this issue). Most of the areas where hydrothermal deposits have been discovered show high backscatter, contrasting with lower values expected from the observed fine-grained sediments and smooth seafloor surfaces apparent on the outer flanks of the caldera (Fig. 6). The high backscatter regions within the floor and close to the walls of the western caldera, that do not correlate with scarps and seafloor roughness, are related to Fe-Mn oxyhydroxide crusts and massive sulfide mineralizations. Similar high backscatter related to hydrothermal vent fields has been observed at the Lucky Strike hydrothermal field of the Mid Atlantic Ridge (Ondreas et al., 2009). Here, backscatter values higher than those of the adjacent areas has been attributed to a rough seafloor surface due to numerous hydrothermal edifices and sulfide debris, including active and dead chimneys (Ondreas et al., 2009).

These observations, including rock magnetization local minima inferred from deep-tow data along the margin of the caldera rim (Caratori Tontini et al., 2013, this issue) and with a wide magnetic local minimum within the caldera derived from the shipborne

data (Fig. 7), suggest widespread hydrothermal alteration in the western sector of the Palinuro volcanic complex. We believe that localization of the hydrothermal systems is probably related to the reactivation of volcanic activity along the caldera ring faults, consistent with the cluster of cones surrounding the floor of the caldera. The formation and reactivation of ring-faults and their susceptibility to intruding ring-dikes may be important for the flow of hydrothermal fluids in these areas and corresponding hydrothermal alteration patterns and ore deposition (e.g., Stix et al., 2003; Beauducel et al., 2004; Embley et al., 2012; Caratori Tontini et al., 2013 this issue).

Seismic reflection, gravity and magnetic data acquired in this study, when combined with high-resolution multibeam and seafloor reflectivity images, provide new insights in the distribution of hydrothermal activity within the central sector of the Palinuro volcanic complex. The distribution of rock magnetization over the two major volcanic cones shows a sharp minimum (with a mean value of ~0 A/m) centred on the flat summit of the larger cone (Fig. 10a). The high frequency components of the magnetic signal in this area indicate both a shallow and sharp variation of seafloor magnetization, suggesting that the area of reduced magnetization is limited to the summit areas of the cones. The volcanic rocks that build-up these edifices should have acquired their magnetization during the present normal geomagnetic field, since the entire volcanic complex is believed to be younger than 0.78 Ma (Colantoni et al. 1981; Beccaluva et al., 1985). Thus, superposition of different volcanic layers with reverse magnetization is an unlikely explanation for the rock magnetization patterns observed. The complete Bouguer anomaly map for the area also shows a minimum centered over the main cone summit (Fig. 10b). The short spatial wavelengths of both gravity and magnetic anomalies cannot be related to deep crustal, or mantle sources, suggesting that

the presence of a low-density and/or low-magnetization region at, or close to, the summit of the main volcanic cone. Hydrothermal alteration of volcanic rocks, with the concomitant formation of secondary mineral phases, can lower the rock density and drastically decrease its magnetization (Caratori Tontini et al., 2010). Hydrothermal related deposits, including Fe-Mn oxyhydroxide crusts and abundant Fe-Mn micronodules, have been recovered from the summits of these two major cones (Rabbi, 1970; Kidd and Armansson, 1979; Dekov and Savelli, 2004). The location of these samples, although rather imprecise (as most were collected during the 70s), suggests that hydrothermal alteration is probably associated with high reflectivity terrains in this general area (Fig. 8). Diver's inspections on the summit of the main cone reported that isolated rocky outcrops rise 1-2 m above biogenic Pleistocene sands (Colantoni et al, 1981), suggesting that the scattered areas of high reflectivity are related to rocky outcrops, whereas low backscatter characterizes biogenic sedimentary cover. Thus, the concentric bands of high backscatter associated with relatively smooth seafloor on the main cone summit may be related to ongoing tectonism associated with ring faults and dikes, which in turn produce a rough seafloor and act as conduits for fluid circulation (Fig. 8). The high backscatter and smooth seafloor in the northwestern sector of the flat summit also suggest an area of possible intense hydrothermal alteration. The flat tops of these two volcanic cones have been subjected to erosion during past sealevel changes (Passaro et al., 2011). In particular, the summit of the main cone was likely strongly reworked during the last sealevel fall and rise in Olocene time. Thus, the hydrothermal deposits located in this area are thought to represent recent hydrothermal activity.

A similar pattern of magnetic anomalies and low rock magnetization is observed for a volcanic structure northeast of the main cone. A multichannel seismic line crossing

this feature shows the internal structure of a collapsed caldera that has a dense network of fractures and faults (Fig. 11). This network, a result of the interaction of volcano-tectonic and regional tectonic structures, promotes sub-seafloor fluid circulation. The collapsed sequence shows enhanced reflection amplitudes relative to those of the adjacent well stratified volcanic sequence. In addition, high backscatter is recorded for this area, despite a relatively smooth seafloor occurring at the bottom of the caldera, while low reflectivity observed on the flanks (Fig. 12). Together, these observations suggest that several hydrothermal deposits may occur within the caldera.

Conclusions

The Marsili seamount represents the axial ridge of the Marsili back-arc basin and is a complex, segmented volcanic structure characterised by volcanic activity along a central ridge and from fissures. The Palinuro volcanic complex consists of several interconnected, superimposed volcanic edifices to form an W-E oriented, 55 km-long continuous volcanic ridge. This complex is located at the northern margin of the Marsili basin, at the boundary between the oceanic basin and the continental slope. Bathymetric and seismic reflection data suggest that structural fabrics trending WNW-ESE, WSW-ENE and ~N-S control the evolution of the volcanic complex, influencing the location and shape of the volcanic edifices. The western sector appears to be the oldest due to a collapsed caldera. The central sector of Palinuro is characterised by younger and larger volcanic cones. The two main cones have flat tops related to erosional processes of lower (past) sealevels, while the easternmost cone has a volcanic crater with a rim that is well preserved. The easternmost sector of Palinuro is structurally controlled by fabrics trending WNW-ESE, with volcanic edifices cut by N-S trending faults.

The Marsili and Palinuro volcanic systems show widespread hydrothermal alteration that correlate with gravity and magnetic lows. Several geophysical parameters enabled us to determine the distribution of hydrothermal alteration and its relationship to both volcanic and tectonic structures, including the role played by ring complexes that favour hydrothermal circulation. The distribution of hydrothermal alteration at Palinuro is mainly related to secondary volcanic structures, such as collapsed calderas and reactivation along ring faults. By contrast, the Marsili ridge shows hydrothermal alteration is largely distributed over the summit area along primary volcanic and tectonic features, similar to systems surveyed along mid-ocean ridges. The different distribution of hydrothermal alteration seen today at Marsili and Palinuro may be attributed to their different tectonic setting, i.e., a back-arc spreading segment (Marsili) and an arc-related volcano (Palinuro), respectively.

Acknowledgments

This work was supported by the Italian Consiglio Nazionale Ricerche and Istituto Nazionale di Geofisica e Vulcanologia. Many people contributed to the success of the research cruises TIR10 and MAVA11 by the R/V *Urania*. We thank C. Doglioni, M. Cuffaro, M. Sacchi, D. Scrocca and the TIR10 scientific party for their collaboration during the expedition. We are particularly indebted to Captain V. Lubrano Lavadera and the officers and crew of the *Urania* for their professionalism and efforts in assuring a successful cruise. A. Cesari and F. Urzi' of SO.PRO.MAR. were very helpful in running the MAVA11 expedition, especially during the sidescan sonar survey. We are grateful to engineer Guido Gay of Gaymarine (http://www.gaymarine.it) for the ROV images. We thank E. Bonatti for helpful discussions.

References

Aliani, S., Bortoluzzi, G., Caramanna, G., and Raffa, F., 2010, Seawater dynamics and environmental settings after november 2002 gas eruption off Bottaro (Panarea, Aeolian Islands, Mediterranean Sea): Continental Shelf Research, v. 30, p. 1338–1348.

Argnani, A., 2009, Evolution of the Southern Tyrrhenian slab tear and active tectonics along the western edge of the Tyrrhenian subducted slab, *in* Van Hinsbergen, D.J.J., Edwards, M.A., and Govers, R., eds., Collision and Collapse at the Africa-Arabia-Eurasia Subduction Zone: Geological Society of London, Special Pubblication, London, v. 311, p. 193–212.

Beauducel, F., De Natale, G., Obrizzo, F., and Pingue, F., 2004, 3-D modelling of Campi Flegrei ground deformations: Role of caldera boundary discontinuities: Pure and Applied Geophysics, v. 161, p. 1329–1344.

Beccaluva, L., Gabbianelli, G., Lucchini, F., Rossi, P.L., and Savelli, C., 1985, Petrology and K/Ar ages of volcanics dregded from the Aeolian seamounts:

implications for geodynamic evolution of the southern Tyrrhenian basin: Earth and Planetary Science Letters, v. 74, p. 187–208.

Bonatti, E., Honnorez, J., Joensuu, O., Rydell, H.S., and Beyth, M., 1972,Submarine iron deposits from the Mediterranean Sea, in Stanley, D.J., The Mediterranean Sea: Hutchinson and Ross, Stroudsburg, Pa., 701–710.

Bortoluzzi, G., Ligi, M., Romagnoli, C., Cocchi, L., Casalbore, D., Sgroi, T., Caratori Contini, F., Cuffaro, M., D'Oriano, F., Ferrante, V., Remia, A., and Riminucci, F., 2010, Interactions between volcanism and tectonics in the Western Aeolian sector, Southern Tyrrhenian Sea: Geophysical Journal Inrenational, v. 183, p. 64–78.

Caratori Tontini, F., Bortoluzzi, G., Carmisciano, C., Cocchi, L., de Ronde, C., Ligi, M., and Muccini, F., 2013, Near-bottom magnetic signatures of submarine hydrotheraml systems at Marsili and Palinuro volcanoes (south Tyrrhenian Sea, Italy): Economic Geology, this issue.

Caratori Tontini, F., Cocchi, L., and Carmisciano, C., 2008, Potential-field inversion for a layer with uneven thickness: the Tyrrhenian Sea density model: Physics of the Earth and Planetary Interiors, v. 166, p. 105–111.

Caratori Tontini, F., Cocchi, L., and Carmisciano, C., 2009, Rapid 3-D forward model of potential fields with application to the Palinuro Seamount magnetic anomaly (southern Tyrrhenian Sea, Italy): Journal of Geophysical Research, v. 114, B02103, doi:10.1029/2008JB005907.

Caratori Tontini, F., Cocchi, L., Muccini, F., Carmisciano, C., Marani, M., Bonatti, E., Ligi, M., and Boschi, E., 2010, Potential-field modeling of collapse-prone submarine volcanoes in the southern Tyrrhenian Sea (Italy): Geophysical Research Letters, v. 37, p. L03305, doi:10.1029/2009GL041757.

Caratori Tontini, F., Davy, B., de Ronde, C.E.J., Embley, R.W., Leybourne, M., and Tivey, M.A., 2012a, Crustal magnetization of Brothers volcano, New Zealand, measured by autonomous underwater vehicles: geophysical expression of a submarine hydrothermal system: Economic Geology, v. 107, p. 1571–1581.

Caratori Tontini, F., de Ronde, C.E.J., Yoerger, D., Kinsey, J.C., and Tivey, M.A., 2012b, 3-D focused inversion of near-seafloor magnetic data with application to the

Brothers volcano hydrothermal system, Southern Pacific Ocean, New Zealand: Journal of Geophysical Research, v. 117, p. B10102, doi:10.1029/2012JB009349.

Cocchi, L., Caratori Tontini, F., Muccini, F., Marani, M. P., Bortoluzzi, G., and Carmisciano, C., 2009, Chronology of the transition from a spreading ridge to an accretional seamount in the Marsili backarc basin (Tyrrhenian Sea): Terra Nova, v. 21, p. 369–374.

Colantoni, P., Lucchini, F., Rossi, P., Sartori, R., and Savelli, C., 1981, The Palinuro volcano and magmatism of the Southeastern Tyrrhenian Sea (Mediterranean): Marine Geology, v. 39, p. 1–12.

D'Agostino, N., and Selvaggi, G., 2004, Crustal motion along the Eurasia-Nubia plate boundary in the Calabrian Arc and Sicily and active extension in the Messina Straits from GPS measurements: Journal of Geophysical Research, v. 109, p. B11402, doi:10.1029/2004JB002998.

De Astis, G., Ventura, G., and Vilardo, G., 2003, Geodynamic significance of the Aeolian volcanism (Southern Tyrrhenian Sea, Italy) in light of structural, seismological, and geochemical data: Tectonics, v. 22, p. 1040, doi:10.1029/2003TC001506.

de Ronde, C.E.J., Massoth, G.J., Butterfield, D.A., Christenson, B.W., Ishibashi, J., Ditchburn, R.G., Hannington, M.D., Brathwaite, R.L., Lupton, J.E., Kamenetsky, V.S., Graham, I.J., Zellmer, G.F., Dziak, R.P., Embley, R.W., Dekov, V.M., Munnik, F., Lahr, J., Evans, L.J., and Takai, K., 2011, Submarine hydrothermal activity and gold-rich mineralization at Brothers volcano, Kermadec arc, New Zealand: Mineralium Deposita, v. 46, p. 541–584.

de Ronde, C.E.J., Faure, K., Bray, C.J., Chappel, D.A., and Wright, I.C., 2003a, Hydrothermal fluids associated with seafloor mineralization at two southern Kermadec arc volcanoes, offshore New Zealand: Mineralium Deposita, v. 38, p. 217–233.

de Ronde, C.E.J., Massoth, G.J., Baker, E.T., and Lupton, J.E., 2003b, Submarine hydrothermal venting related to volcanic arcs: Society of Economic Geologists, Special Publications, v. 10, p. 91–110.

Dekov, V.M., Kamenov, G.D., Savelli, C., and Stummeyer, J., 2006, Anthropogenic Pb component in hydrothermal ochres from Marsili Seamount (Tyrrhenian Sea): Marine Geology, v. 229, p. 199–208.

Dekov, V.M., Kamenov, G.D., Savelli, C., Stummeyer, J., Thiry, M., Shanks, W., Willingham, A., Boycheva, T. B., Rochette, P., Kuzmann, E., Fortin, D., and Vertes, A., 2009, Metalliferous sediments from Eolo Seamount (Tyrrhenian Sea): Hydrothermal deposition and re-deposition in a zone of oxygen depletion: Chemical Geology, v. 264, p. 347–363.

Dekov, V.M., Kamenov, G.D., Stummeyer, J., Thiry, M., Savelli, C., Shanks, W.C., Fortin, D., Kuzmann, E., and Vertes, A., 2007, Hydrothermal nontronite formation at Eolo Seamount (Aeolian volcanic arc, Tyrrhenian Sea): Chemical Geology, v. 245, p. 103–119.

Dekov, V.M., and Savelli, C., 2004, Hydrothermal activity in the SE Tyrrhenian Sea: an overview of 30 years of research: Marine Geology, v. 204, p. 161–185.

Doglioni, C., 1991, A proposal kinematic modelling for W-dipping subductions - possible applications to the Tyrrhenian-Apennine systems: Terra Nova, v. 3, p. 423–434.

Doglioni, C., Innocenti, F., Morellato, C., Procaccianti, D., and Scrocca, D., 2004, On the Tyrrhenian sea opening: Memorie Descrittive della Carta Geologica d’Italia, v. 64, p. 147–164.

Doglioni, C., Ligi, M., Scrocca, D., Bigi, S., Bortoluzzi, G., Carminati, E., Cuffaro, M., D'Oriano, F., Forleo, V., Muccini, F., and Riguzzi, F., 2012, The tectonic puzzle of the Messina area (Southern Italy): Insights from new seismic reflection data: Scientific Reports, v. 2, p. 970, doi:10.1038/srep00970.

Doglioni, C., Merlini, S., and Cantarella, G., 1999, Foredeep Geometries at the front of the Apennines in the Ionian Sea (central Mediterranean): Earth and Planetary Science Letters, v. 168, p. 243–254.

Eckhardt, J.-D, Glasby, G.P., Puchelt, H., and Berner, Z., 1997, Hydrothermal Manganese crusts from Enarete and Palinuro Seamounts in the Tyrrhenian Sea: Marine Georesources and Geotechnology, v. 15, p. 175–208.

Embley, R.W., de Ronde, C.E.J., Merle, S.G., Davy, B., and Caratori Tontini, F., 2012, Detailed Morphology and Structure of an Active Submarine Arc Caldera: Brothers Volcano, Kermadec Arc: Economic Geology, v. 107, p. 1557–1570.

Faccenna, C., Mattei, M., Funiciello, R., and Jolivet, L., 1997, Styles of back-arc extension in the Central Mediterranean: Terra Nova, v. 9, p. 126–130.

Gamberi, F., Marani, M., and Savelli, C., 1997, Tectonic, Volcanic and Hydrothermal Features of a Submarine Portion Of The Aeolian Arc (Tyrrhenian Sea): Marine Geology, v. 140, p. 167–181.

Grauch, V.J.S., and Johnston, C.S., 2002, Gradient window method: A simple way to separate regional from local horizontal gradients in gridded potential-field data: In Technical Program Expanded Abstracts, Society of Exploration Geophysicists, p. 762–765, 72nd Annual Meeting.

Hannington, M.D., Jonasson, I.R., Herzig, P.M., and Petersen, S., 1995, Physical and chemical processes of seafloor mineralization at midocean ridges, *in* Humphris, S.E., Zierenberg, R.A., Mullineaux, L.S., and Thomson, R.E., eds., Seafloor hydrothermal systems:Physical, chemical, biological and geological interactions: American Geophysical Union, Geophysical Monograph, v. 91, p. 115–157.

Ishibashi, J., and Urabe, T., 1995, Hydrothermal activity related to arc-backarc magmatism in the Western Pacific, *in* Taylor, B., ed., Backarc basins: tectonics and magmatism: Plenum Publishing Corp., New York, p. 451–495.

Kastens, K., Mascle, J., Auroux, C.A., Bonatti, E., Broglia, C., Channell, J., Curzi, P., Emeis, K., Glacon, G., Hasegawa, S., Hieke, W., Mascle, G., McCoy, F., McKenzie, J., Mendelson, J., Mueller, C., Rehault, J., Robertson, A., Sartori, R., Sprovieri, R., and Tori, M., 1988, ODP leg 107 in the Tyrrhenian Sea; insights into passive margin and back-arc basin evolution: Geological Society of America Bulletin, v. 100, p. 1140–1156.

Kidd, R.B., and Armansson, H., 1979, Manganese and iron micronodules from a volcanic seamount in the Tyrrhenian Sea: Journal of the Geological Society of London, v. 136, p. 71–76.

Klaucke, I., Masson, D.G., Petersen, C.J., Weinrebe, W., and Ranero, C.R., 2008,

Multi-frequency geoacoustic imaging of fluid escape features offshore Costa Rica: implications for the quantification of seep processes: Geochemistry Geophysics Geosystems, v. 9, p. Q04010, doi:10.1029/2007GC001708.

Ligi, M., and Bortoluzzi, G., 1989, PLOTMAP: geophysical and geological applications of good standard quality cartographic software: *Computers and Geosciences*, v. 15, p. 519–585.

Lupton, J., de Ronde, C.E.J., Sprovieri, M., Baker, E.T., Bruno, P.P., Italiano, F., Walker, S., Faure, K., Leybourne, M., Britten, K., and Green, R., 2011, Active hydrothermal discharge on the submarine Aeolian Arc: J. Geophy. Res., v. 116, p. B02102, doi:10.1029/2010JB007738.

Malinverno, A., and Ryan, W.B.F., 1986, Extension in the Tyrrhenian sea and shortening in the Apennines as result of arc migration driven by sinking of the lithosphere: Tectonics, v. 5, p. 227–245.

Mantovani, E., Albarello, D., Tamburelli, C., and Babbucci, D., 1996, Evolution of the Tyrrhenian Basin and surrounding regions as a result of the Adrica-Eurasia convergence: Journal of Geodynamics, v. 21, p. 35–72.

Marani, M.P., and Gamberi, F., 2004, Distribution and nature of submarine volcanic landforms in the Tyrrhenian sea : the arc vs the backarc, *in* Marani, M. P., Gamberi, F., and Bonatti, E., eds., From seafloor to deep mantle: architecture of the Tyrrhenian backarc basin: APAT, Memorie Descrittive Carta Geologica d'Italia, v. 64, p. 109–126.

Marani, M.P., Gamberi, F., Bortoluzzi, G., Carrara, G., Ligi, M., and Penitenti, D., 2004, Tyrrhenian sea bathymetry, *in* Marani, M.P., Gamberi, F., and Bonatti, E., eds., From seafloor to deep mantle: architecture of the Tyrrhenian backarc basin, APAT, Memorie Descrittive Carta Geologica d'Italia, v. 44, p. 1–195.

Marani, M.P., Gamberi, F., Casoni, L., Carrara, G., Landuzzi, V., Musacchio, M., Penitenti, D., Rossi, L., and Trua, T., 1999, New rock and hydrothermal samples from the southern Tyrrhenian sea: MAR-98 research cruise: Giornale di Geologia, v. 61, p. 3–24.

Marani, M.P., and Trua, T., 2002, Thermal constriction and slab tearing at the origin of

a superinflated spreading ridge: Marsili volcano (Tyrrhenian Sea): Journal of Geophysical Research, v. 107, p. 2188, doi:10.1029/2001JB000285.

Minniti, M., and Bonavia, F., 1984, Copper-ore grade hydrothermal mineralization discovered in a seamount in the Tyrrhenian Sea (Mediterranean): is the mineralization related to porphyry copper or to base metal lodes?: Marine Geology, v. 59, p. 271–282.

Monecke, T., Petersen, S., Lackschewitz, K., Huegler, M., Hannington, M., and Gemmell, J., 2009, Shallow submarine hydrothermal systems in the Aeolian Volcanic Arc, Italy: Eos, Transaction of American Geophysical Union, v. 90, p. 110–111.

Nicolosi, I., Speranza, F., and Chiappini, M., 2006, Ultrafast oceanic spreading of the Marsili Basin, southern Tyrrhenian Sea: Evidence from magnetic anomaly analysis: Geology, v. 34, p. 717-720.

Ondreas, H., Cannat, M., Fouquet, Y., Normand, A., Sarradin, P-M., and Sarrazin, J., 2009, Recent volcanic events and the distribution of hydrothermal venting at the Lucky Strike hydrothermal field, Mid-Atlantic Ridge: Geochemistry Geophysics Geosystems, v. 10, p. 1–18.

Paltrinieri, D., Signanini, P., Viezzoli, C., Di Sabatino, B., Madonna, R., Torrese, P., Rainone, M.L., Rusi, S., Marino, A., Caso, C., Vitale, S., Iezzi, B., Bortoluzzi, G., Ferrante, V., Redini, F., Rovere, M., Caratori Tontini, F., Cocchi, L., Muccini, F., D'Anna, G., Mangano, G., Calcara, M., Cuoco, E., Troppa, F., Siena, P., 2006, Joint Research Project "PROMETHEUS" an Integrated Study of the Marsili SMT., Thyrrhenian Sea. Report on the morphobathymetric, magnetometric, gravimetric, CTD water and bottom sampling investigations during cruise MRS06 aboard R/V Universitatis: ricerca.ismar.cnr.it/CRUISE_REPORTS/2000-2009/MRS06_REP/MRS06_REP.pdf.

Parker, R., 1973, The rapid calculation of potential anomalies: Geophysical Journal of Royal Astronomical Society, v. 31, p. 447–455.

Passaro, S., Milano, G., D'Isanto, C., Ruggieri, S., Tonielli, R., Bruno, P., Sprovieri, M., and Marsella, E., 2010, DTM-Based morphometry of the Palinuro seamount

(Italy, Eastern Tyrrhenian Sea): geomorphological and volcanological implication: Geomorphology, v. 115, p. 129–140.

Passaro, S., Milano, G., Sprovieri, M., Ruggieri, S., and Marsella, E., 2011, Quaternary still-stand landforms and relations with flank instability events of the Palinuro Bank (southeastern Tyrrhenian Sea): Quaternary International, v. 232, p. 228–237.

Patacca, E., Sartori, R., and Scandone, P., 1990, Tyrrenian basin and apenninic arcs: kinematic relations since late Tortonian time: Memorie della Società Geologica Italiana, v. 45, p. 425–451.

Peters, M., Strauss, H., Petersen, S., Kummer, N., and Thomazo, C., 2011, Hydrothermalism in the Tyrrhenian Sea: inorganic and microbial sulfur cycling as revealed by geochemical and multiple sulfur isotope data: Chemical Geology, v. 280, p. 217–231.

Petersen, S., and Monecke, T., 2009, RV METEOR Cruise Report M73/2: Shallow drilling of hydrothermal sites in the Tyrrhenian Sea: Report of the Leibniz- Institute of Marine Sciences at the Christian Albrechts University Kiel, v. 30, 230 p.

Petersen, S., Monecke, T., Augustin, N., De Benedetti, A., Esposito, A., Gartner, A., Gardeler, A., Gemmell, J., Gibson, H., He, G., Huegler, M., Kayser, A., Kleeberg, R., Kver, J., Kummer, N., Lackschewitz, K., Lappe, F., Perrin, K., Peters, M., Sharpe, R., Simpson, K., Smith, D., and Wan, B., 2008, Drilling submarine hydrothermal systems in the Tyrrhenian Sea, Italy: InterRidge News, v. 17, p. 21–23.

Petersen, S., Monecke, T., Westhues, A., Hannington, M.D., Bruce Gemmel, J., Sharpe, R., Peters, M., Strauss, A., Lackschewitz, K., Augustin, N., Gibson, H., and Kleeberg, 2013, Drilling shallow-water massive sulfides at the Palinuro volcanic complex, Aeolian Island Arc, Italy: Economic Geology, this issue.

Pirajno, F., 2010, Hydrothermal Processes and Mineral Systems: Springer, 1250 p.

Rabbi, E., 1970, Ricerche chimiche e geochimiche, *in* Selli, R., ed., Ricerche Geologiche Preliminari nel Mar Tirreno: Giornale di Geologia, v. 37, p. 109–128.

Royden, L., 1988, Flexural behavior of the Continental Lithosphere in Italy Constraints imposed by gravity and deflection data: Journal of Geophysical Research, v. 93, p.

7747–7766.

Skinner, B.J., 1983, Submarine volcanic exhalations that form mineral deposits: an old idea now proven correct, *in* Rona, P.A., Bostrom, K., Laubier, L., and Smith, K.L., eds., Hydrothermal processes at seafloor spreading centers: NATO Conference Series IV, Plenum Publishing Corp., New York, v. 12, p. 557–570.

Sprovieri, M., Passaro, S., Marsella, E., Bruno, P., Baker, E. T., de Ronde, C. E., Anzalone, E., Britten, K., Crisafi, F., Core, M. D., Di Martino, G., D'Isanto, C., Faure, K., Gherardi, S., Innangi, S., Italiano, F., Cono, V. L., Leybourne, M., Lupton, J. E., Milano, G., Prevedello, L., Punzo, M., Ruggieri, S., Sammartino, S., Scotto di Vettimo, P., Spada, L., Tamburrino, S., Tonielli, R., Mattia Vallefuoco, R. V., and Walker, S. L., 2008, Campagna Oceanografica AEOLIAN 2007 Rapporto Attività: eprints.bice.rm.cnr.it/1243/1/RT AEOLIAN07.pdf.

Stix, J., Kennedy, B., Hannington, M., Gibson, H., Fiske, R., Mueller, W., and Franklin, J., 2003, Caldera-forming processes and the origin of submarine volcanogenic massive sulfide deposits: Geology, v. 31, p. 375–378.

Tivey, M.A., and Dyment, J., 2010, The magnetic signature of hydrothermal systems in slow spreading environments, *in* Rona, P.A., Devey, C.W, Dyment, J., and Murton, B.J., eds., Diversity of hydrothermal systems on slow spreading ridge: American Geophysical Union, Geophysical Monograph Series, v. 188, p. 43–66.

Trua, T., Marani, M. P., and Gamberi, F., 2011, Magmatic evidence for African mantle propagation into the southern Tyrrhenian backarc region: Geological Society of America Special Papers, v. 478, p. 283–305.

Tufar, W., 1991, Paragenesis of complex massive sulfide ores from the Tyrrhenian Sea: Mitteilungen der Osterreich ischen Geologischen Gesellschaft, v. 84, p. 265–300.

Ventura, G., Milano, G., Passaro, S., and Sprovieri, M., 2012, The Marsili Ridge (Southern Tyrrhenian Sea, Italy): An island-arc volcanic complex emplaced on a 'relict' back-arc basin: Earth-Science Reviews, v. 116, p. 85–94.

Wallace, P.J., 2005, Volatiles in subduction zone magmas: concentrations and fluxes based on melt inclusion and volcanic gas data: Journal of Volcanology and Geothermal Research, v. 140, p. 217–240.

Wessel, P. and Smith, W.H.F., 1995, New version of the Generic Mapping Tools released: EOS, Transaction of American Geophysical Union, v. 76, p. 329.

Woodward, D.J., and Mumme, T.C., 1993, Variation of magnetization on White Island, New Zealand: New Zealand Journal of Geology and Geophysics, v. 36, p. 447–451.

FIGURE CAPTIONS

Figure 1. Bathymetry of the southern Tyrrhenian Sea (data from Marani et al. (2004). The numbered boxes indicate the figures related to the volcanic edifices covered by this study (i.e., Marsili and Palinuro volcanic complexes). The inset shows a schematic representation of the tectonics affecting southern Italy (after D'Agostino & Selvaggi, 2004).

Figure 2. Marsili volcanic complex. **A** Shaded relief image derived from multibeam bathymetry. Illumination from the NNE. The box outlines the location of morphological details shown in Figure 3. **B** Multibeam reflectivity. **C** Complete Bouguer anomaly map obtained by merging data from this study (cruise MAVA11) with those collected during previous expeditions. **D** Horizontal magnetic gradient along a 108° N direction (i.e., perpendicular to the ridge axis) after removing the regional gradient in order to minimize high relief effects of Marsili ridge. The gradiometer data were collected during the 2006 PROMETHEUS cruise (Paltrinieri et al., 2006). Bathymetric contour intervals are 50 m. Hydrothermal deposits are indicated by blue stars (vents) and red filled squares (Fe-Mn oxyhydroxides and massive sulfides). $^{3}He/^{4}He$ anomalies from active vent sites are from Lupton et al. (2011) and are given by the yellow filled circles.

Figure 3. High resolution multibeam bathymetry of the summit region of Marsili ridge. Bathymetric contour intervals are 25 m. Hydrothermal

deposits are given by the same symbols as in Figure 2. Red solid lines indicate lineaments and/or faults.

Figure 4. ROV images of hydrothermal chimneys observed along the crest of Marsili ridge. Vent locations are shown in Figure 3.

Figure 5. Map showing the distribution of the main volcanic, structural and sedimentary features of the Palinuro volcanic complex. The labelled dashed boxes indicate the three sectors of the volcanic complex: *W*, western; *C*, central; and *E*, eastern. The numbered boxes refer to other figures of the volcanic complex given in this paper.

Figure 6. Western sector of the Palinuro volcanic complex. **A** Shaded relief image derived from multibeam bathymetry. Illuminated from the NNE. **B** Multibeam reflectivity. Bathymetric contour intervals are 20 m. Hydrothermal deposit locations taken from Colantoni et al. (1981), Eckhardt et al. (1997), Minniti and Bonavia (1984), Peterson et al. (2008), Monecke et al. (2009) and Peters et al. (2011). $^{3}He/^{4}He$ anomalies from Lupton et al. (2011) are also shown (symbols as in Fig. 2).

Figure 7. Western sector of the Palinuro volcanic complex. **A** Map of the reduced-to-pole magnetic anomaly. **B** Map of the complete Bouguer gravity anomaly. Bathymetric contour intervals are 20 m. Symbols for the various hydrothermal deposits given in Figure 2.

Figure 8. Central sector of the Palinuro volcanic complex. **A** Shaded relief image derived from multibeam bathymetry. Illuminated from the

NNE. **B** Multibeam reflectivity. Bathymetric contour intervals are 20 m. Hydrothermal deposits taken from Colantoni et al. (1981) and Eckhardt et al. (1997); $^{3}He/^{4}He$ anomalies from Lupton et al. (2011) are also indicated (symbols as in Fig. 2).

Figure 9. Central-Eastern area of Palinuro seamount. Multibeam bathymetry data was obtained by merging the data from this study (cruise MAVA11) with those of Marani et al. (2004). Contour interval 100 m. The yellow solid line shows the shot locations of the multichannel seismic line TIR10/12, as shown in Figure 11. Hydrothermal deposits and $^{3}He/^{4}He$ anomalies from Lupton et al. (2011) are also shown (symbols as in Fig. 2).

Figure 10. Magnetic and gravity maps for the Central-Eastern area of Palinuro seamount. **A** Map of the magnetization obtained by inversion of reduced-to-pole magnetic anomalies. **B** Map of the complete Bouguer gravity anomaly. Bathymetric contour interval 20 m. Symbols as in Figure 2.

Figure 11. Depth migrated section of seismic line TIR10/12. **A** Processed data only; **B** interpretation of the processed data. Red lines mark faults and fractures. F_1 and F_2 are two main regional faults that intersect with local volcano-tectonic features. Location of the seismic line is shown in Figure 9.

Figure 12. Northern-eastern part of the central sector, Palinuro volcanic complex. **A** Multibeam bathymetry (contour interval 50 m), **B** reflectivity, and

C sub-bottom profile (CHIRP) and reduced-to-pole magnetic anomaly (solid red line) along seismic line TIR10/12.

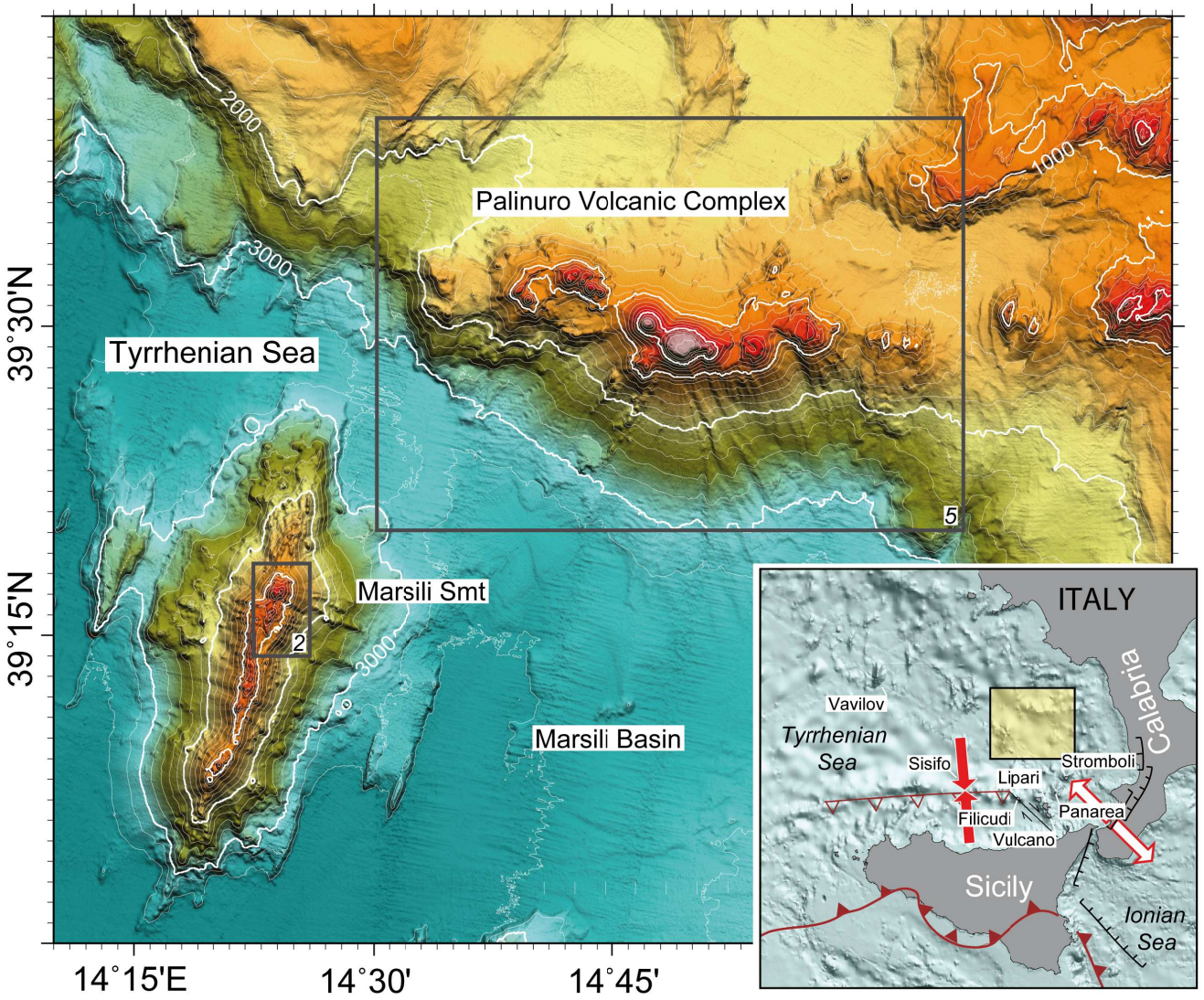
Palinuro Volcanic Complex
Tyrrhenian Sea
Marsili Smt
Marsili Basin
2000
3000
1000
3000
5
2
39°30'N
39°15'N
14°15'E
14°30'
14°45'
ITALY
Calabria
Vavilov
Tyrrhenian Sea
Sisifo
Lipari
Stromboli
Filicudi
Panarea
Vulcano
Sicily
Ionian Sea

Figure 1

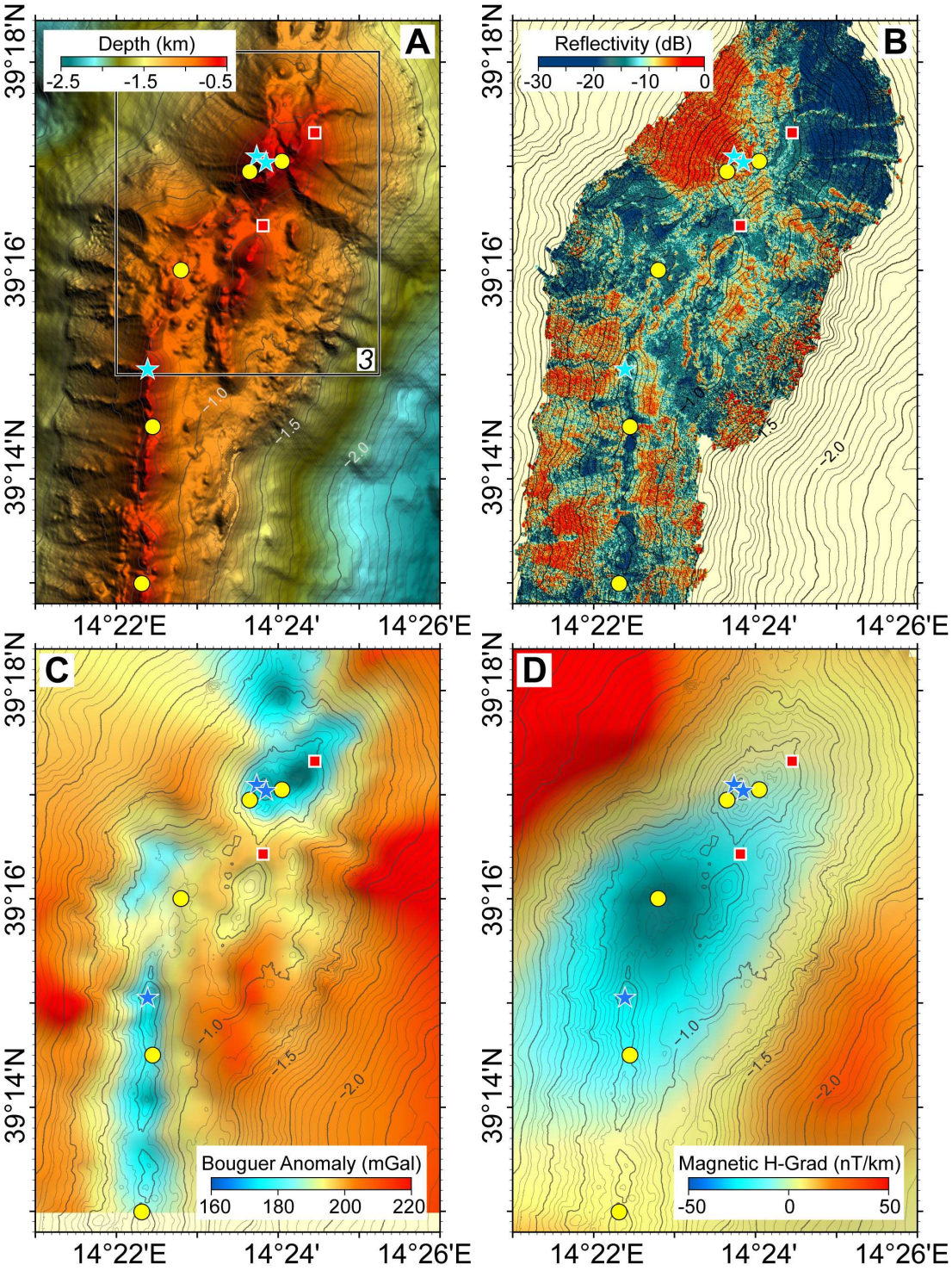
A
Depth (km)
-2.5
-1.5
-0.5
3
B
Reflectivity (dB)
-30
-20
-10
0
C
Bouguer Anomaly (mGal)
160
180
200
220
D
Magnetic H-Grad (nT/km)
-50
0
50
39°18'N
39°16'
39°14'N
14°22'E
14°24'
14°26'E

Figure 2

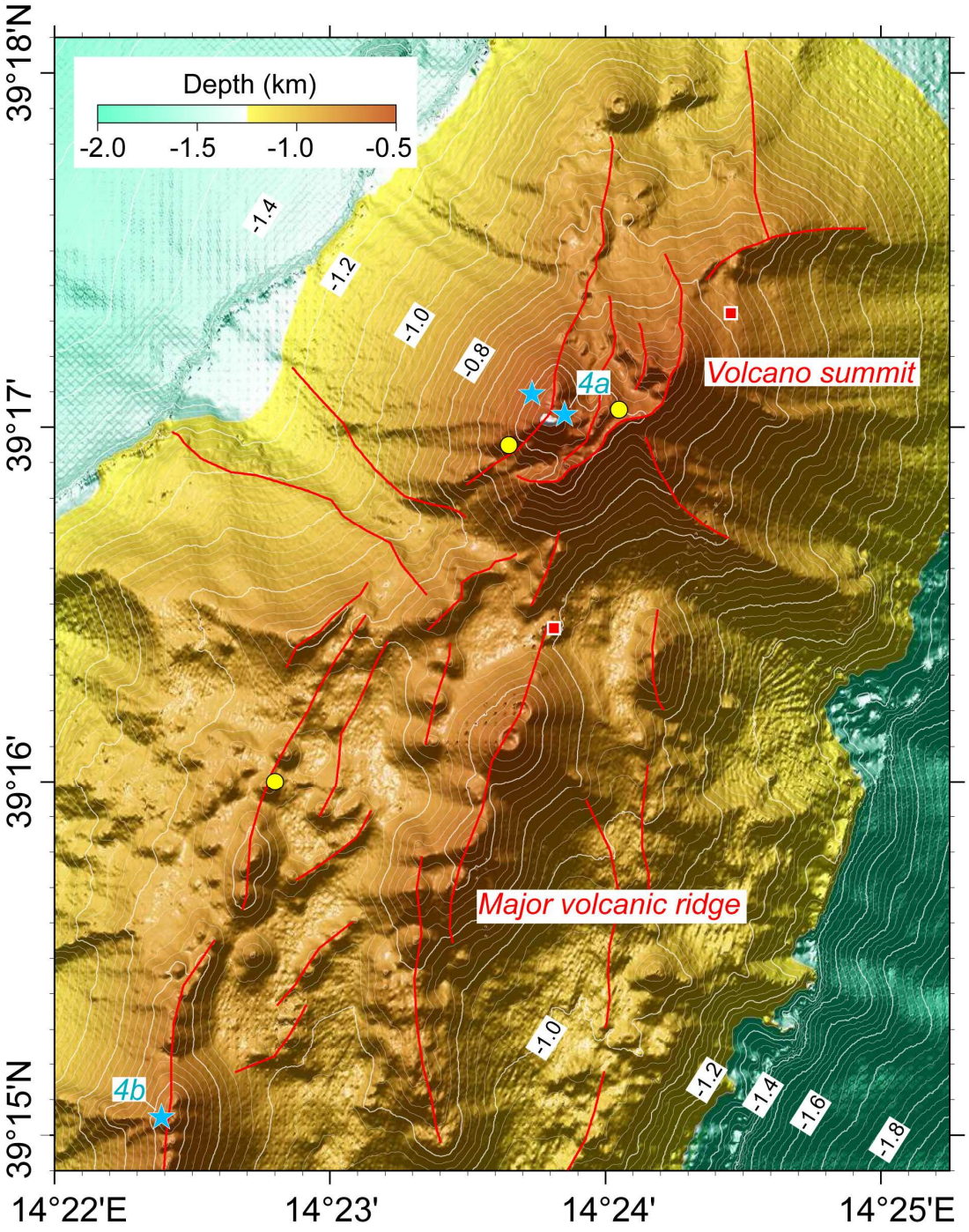
Depth (km)
-2.0
-1.5
-1.0
-0.5
-1.4
-1.2
-1.0
-0.8
Volcano summit
4a
Major volcanic ridge
-1.0
-1.2
-1.4
-1.6
-1.8
4b
39°18'N
39°17'
39°16'
39°15'N
14°22'E
14°23'
14°24'
14°25'E

Figure 3

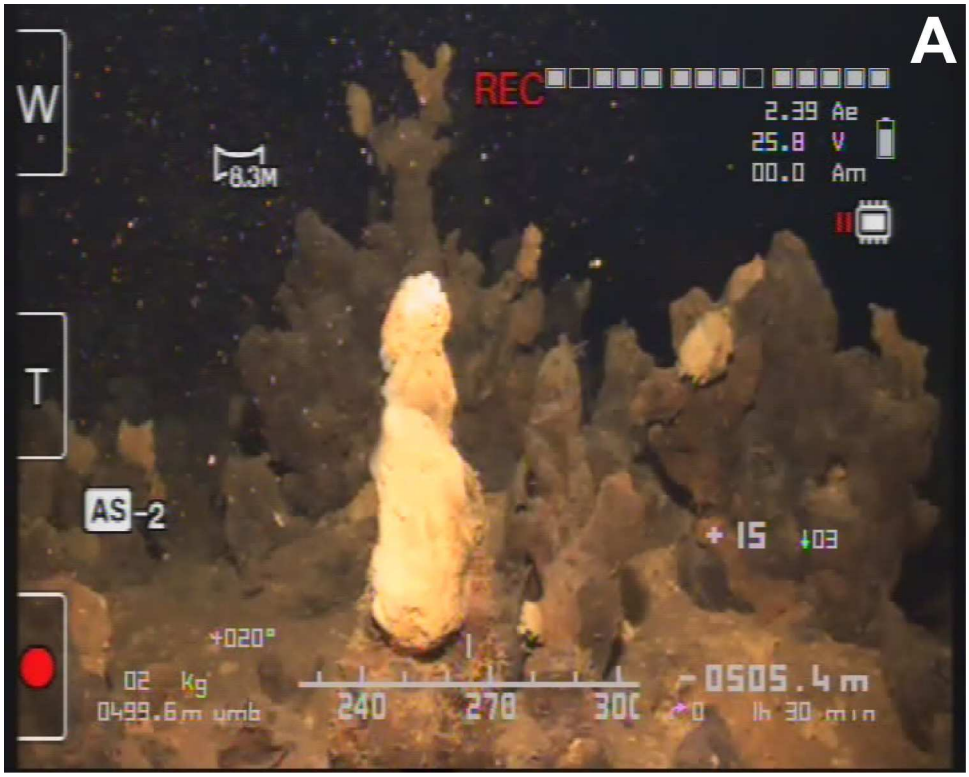
A
W
T
REC
2.39 Ae
25.8 V
00.0 Am
8.3M
AS-2
+15
+020°
02 kg
0499.6m umb
240
270
0505.4m
1h 30 min


B
W
T
REC
2.43 Ae
25.4 V
00.0 Am
8.3M
AS-2
+12
01 kg
0645.3m umb
60
90
120
0660.1m
0h 41 min

Figure 4

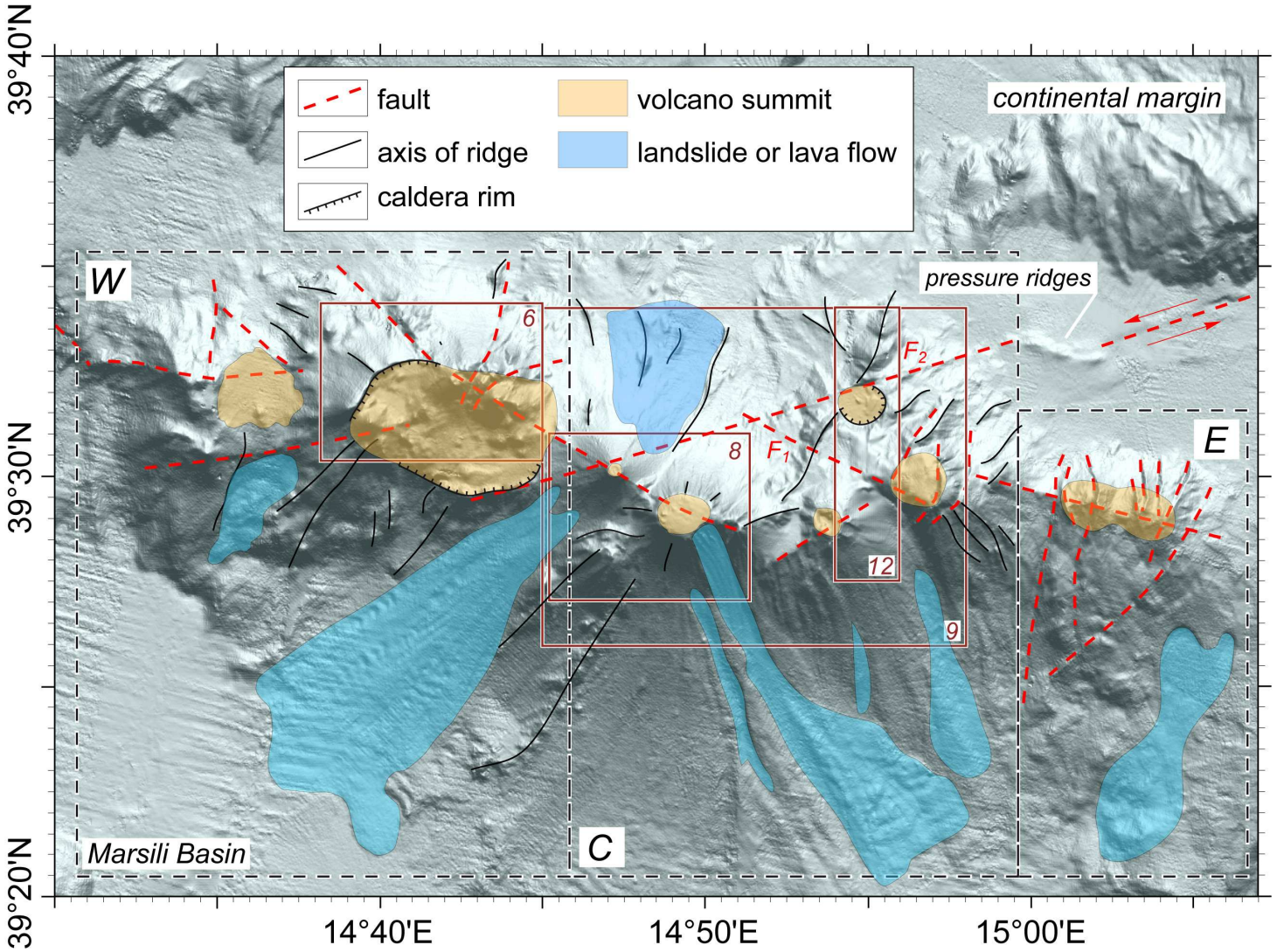
fault
axis of ridge
caldera rim
volcano summit
landslide or lava flow
continental margin
pressure ridges
W
C
E
6
8
9
12
F_1
F_2
Marsili Basin
39°40'N
39°30'N
39°20'N
14°40'E
14°50'E
15°00'E

Figure 5

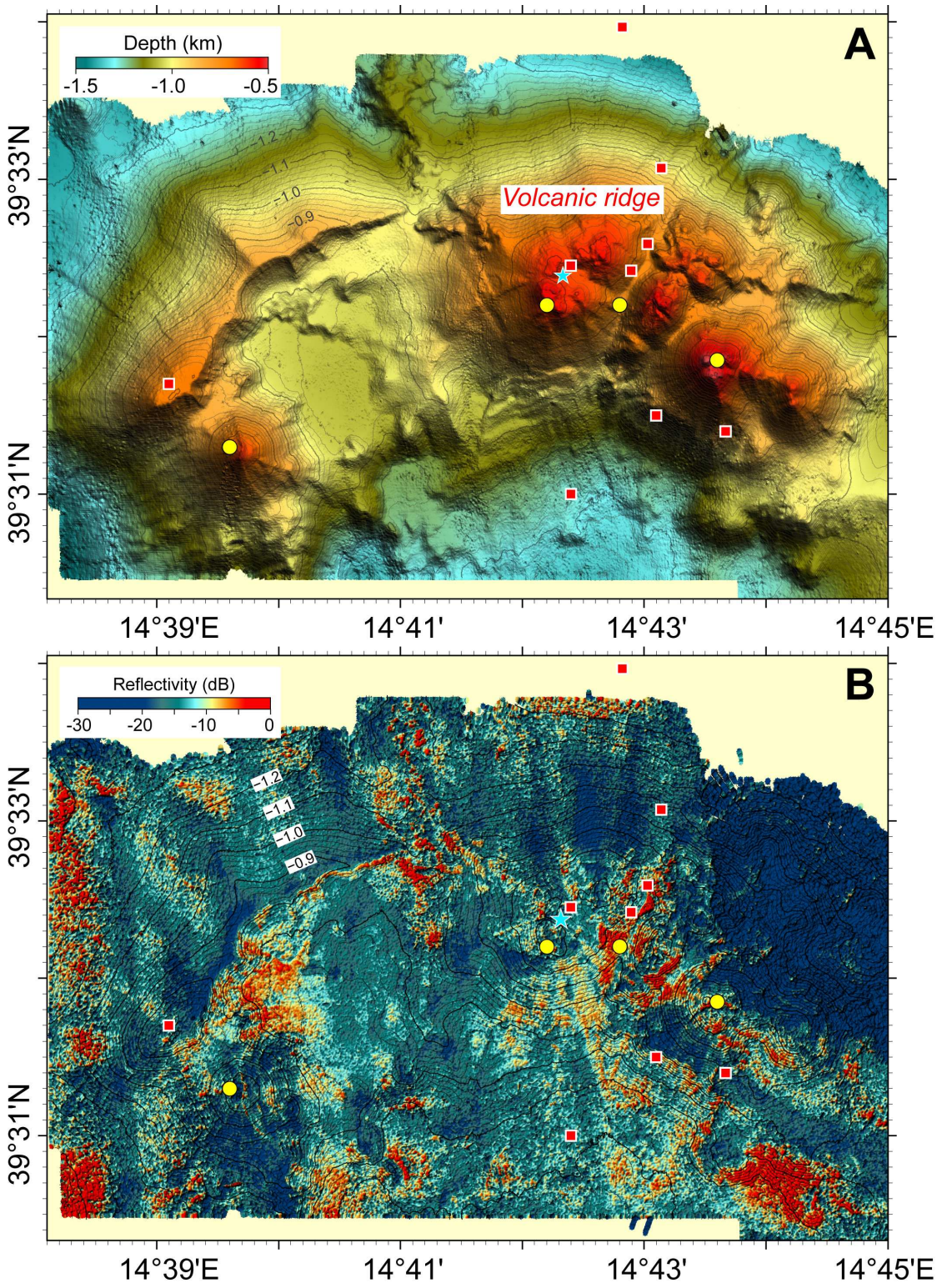
A
Depth (km)
-1.5
-1.0
-0.5
Volcanic ridge
-1.2
-1.1
-1.0
-0.9
39°33'N
39°31'N
14°39'E
14°41'
14°43'
14°45'E
B
Reflectivity (dB)
-30
-20
-10
0
-1.2
-1.1
-1.0
-0.9
39°33'N
39°31'N
14°39'E
14°41'
14°43'
14°45'E

Figure 6

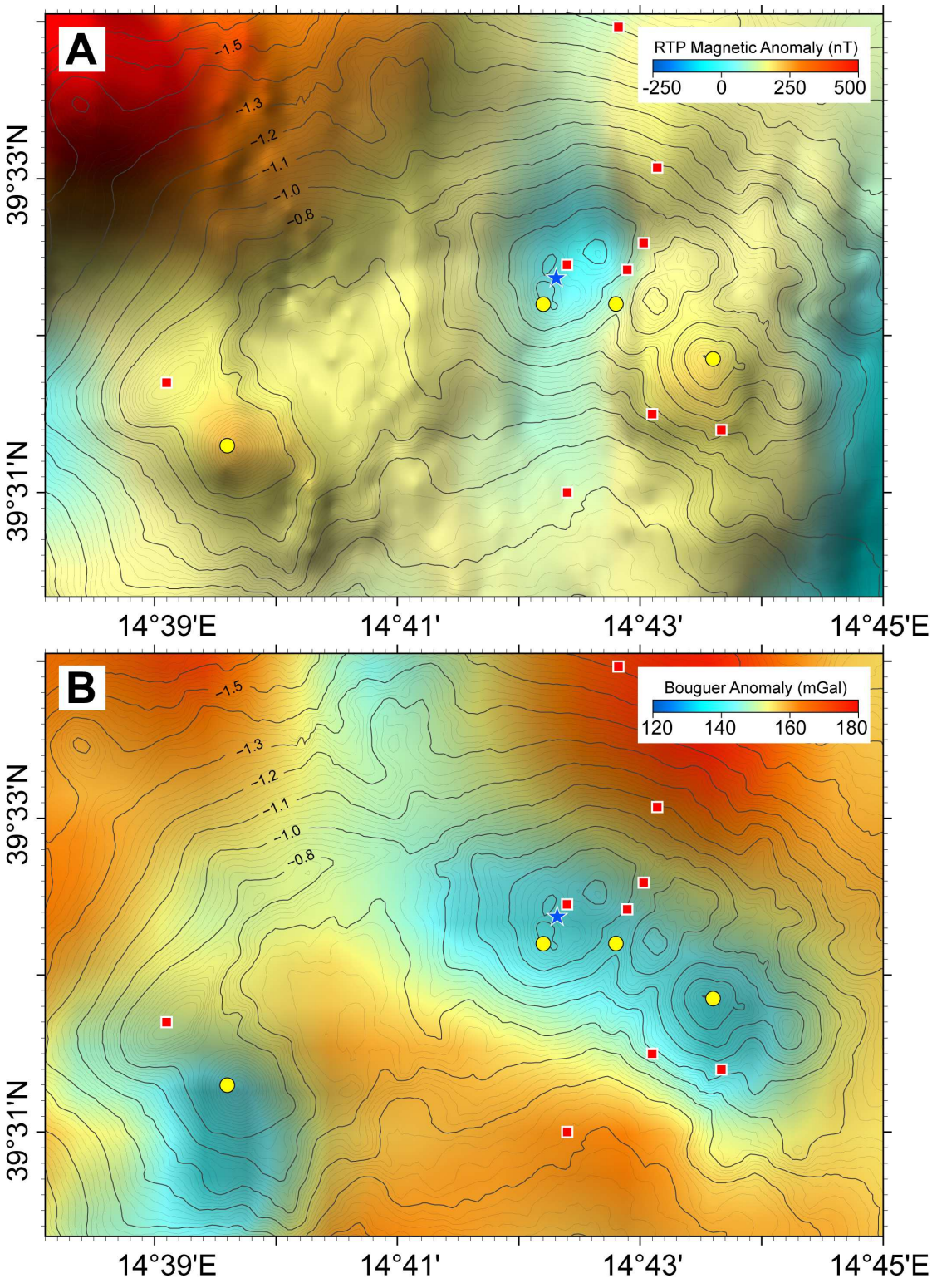
A
RTP Magnetic Anomaly (nT)
-250
0
250
500
-1.5
-1.3
-1.2
-1.1
-1.0
-0.8
39°33'N
39°31'N
14°39'E
14°41'
14°43'
14°45'E
B
Bouguer Anomaly (mGal)
120
140
160
180
-1.5
-1.3
-1.2
-1.1
-1.0
-0.8
39°33'N
39°31'N
14°39'E
14°41'
14°43'
14°45'E

Figure 7

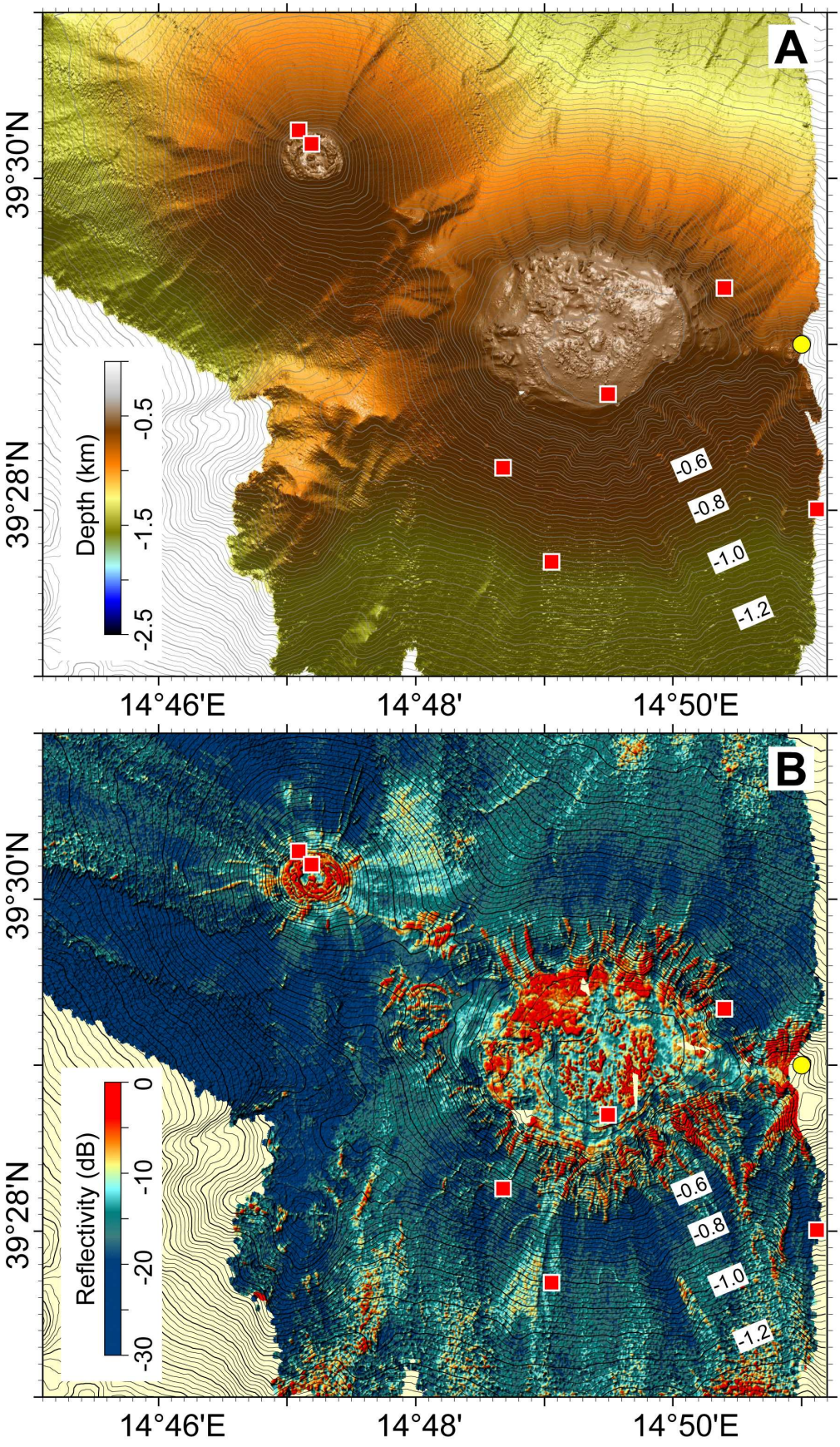
A
B
39°30'N
39°28'N
14°46'E
14°48'
14°50'E
Depth (km)
-0.5
-1.5
-2.5
Reflectivity (dB)
0
-10
-20
-30
-0.6
-0.8
-1.0
-1.2

Figure 8

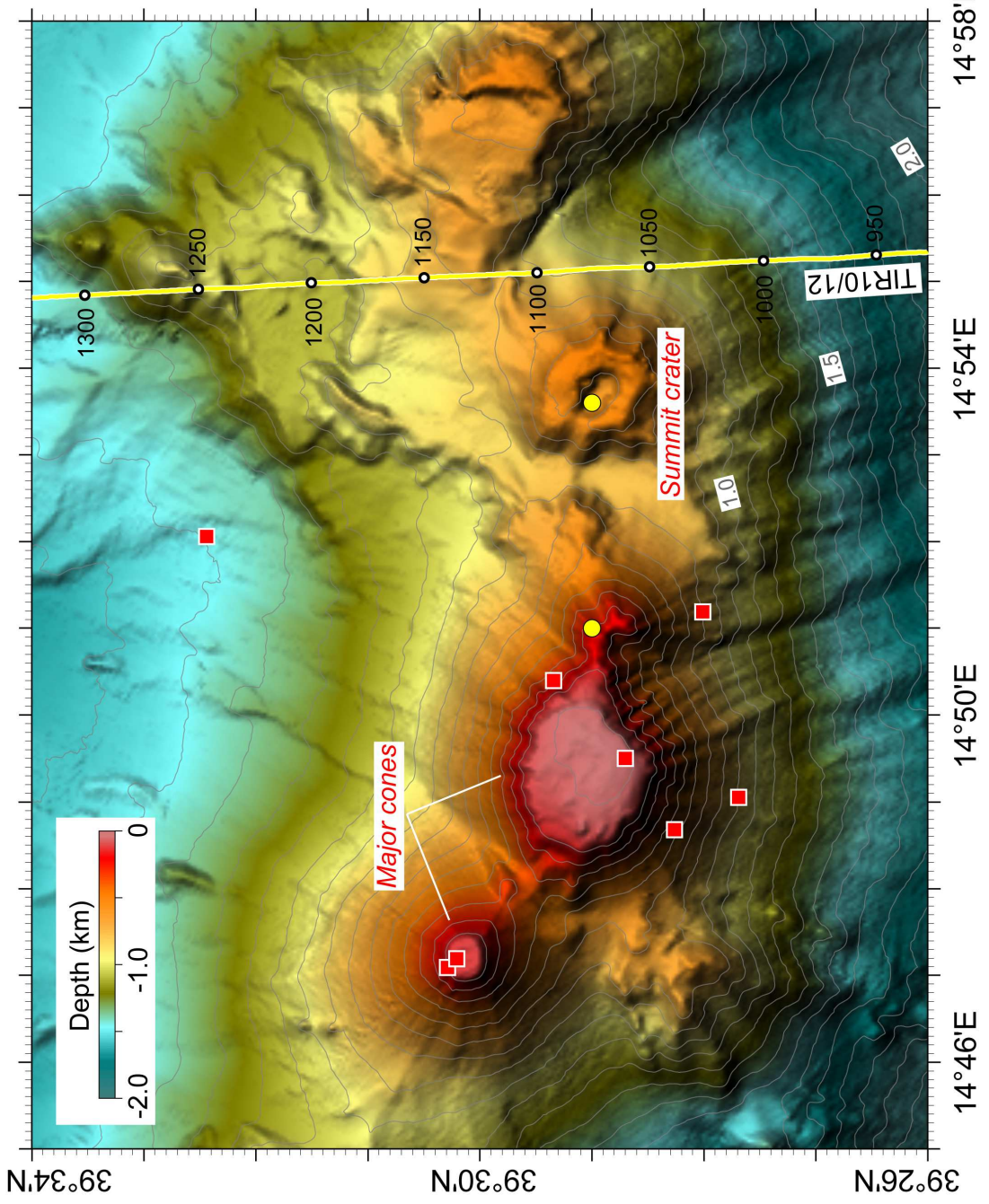
39°34'N
39°30'N
39°26'N
14°46'E
14°50'E
14°54'E
14°58'E
Depth (km)
0
-1.0
-2.0
Major cones
Summit crater
TIR10/12
1300
1250
1200
1150
1100
1050
1000
950
0.5
1.0
1.5
2.0

Figure 9

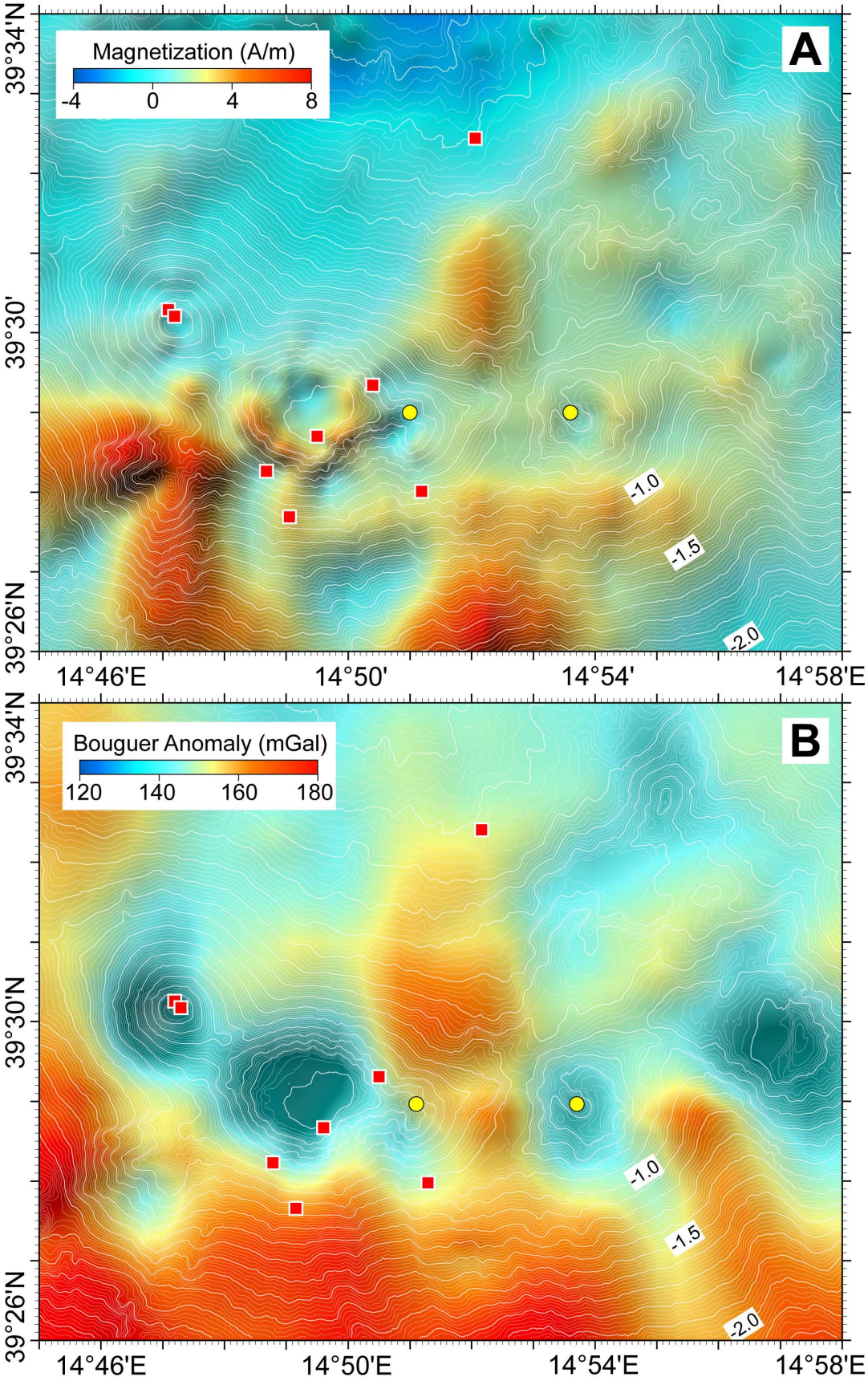
Magnetization (A/m)
-4
0
4
8
A
39°34'N
39°30'
39°26'N
14°46'E
14°50'
14°54'
14°58'E
-1.0
-1.5
-2.0
Bouguer Anomaly (mGal)
120
140
160
180
B
39°34'N
39°30'N
39°26'N
14°46'E
14°50'E
14°54'E
14°58'E
-1.0
-1.5
-2.0

Figure 10

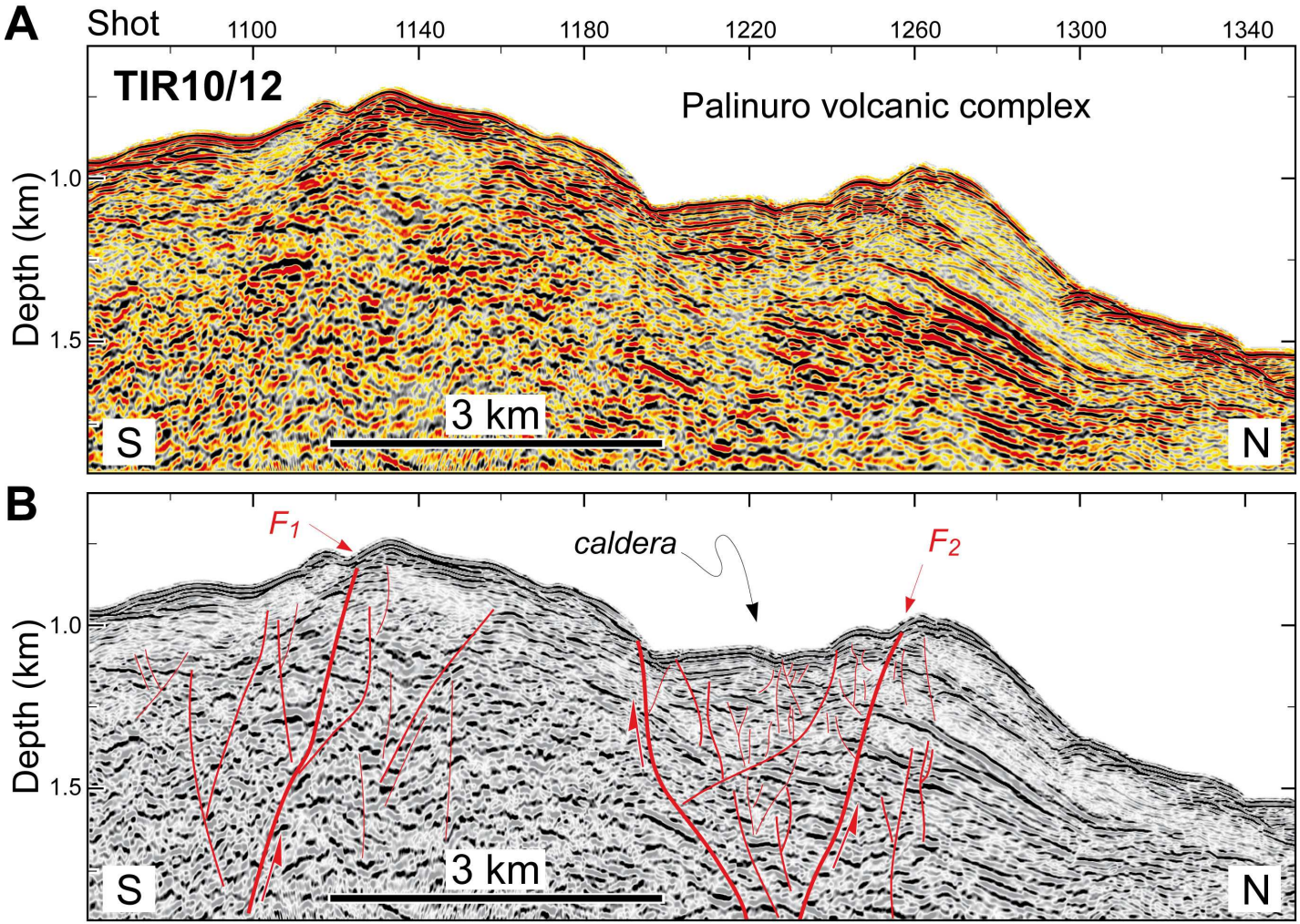
A
Shot
1100
1140
1180
1220
1260
1300
1340
TIR10/12
Palinuro volcanic complex
Depth (km)
1.0
1.5
3 km
S
N
B
F1
caldera
F2
Depth (km)
1.0
1.5
3 km
S
N

Figure 11

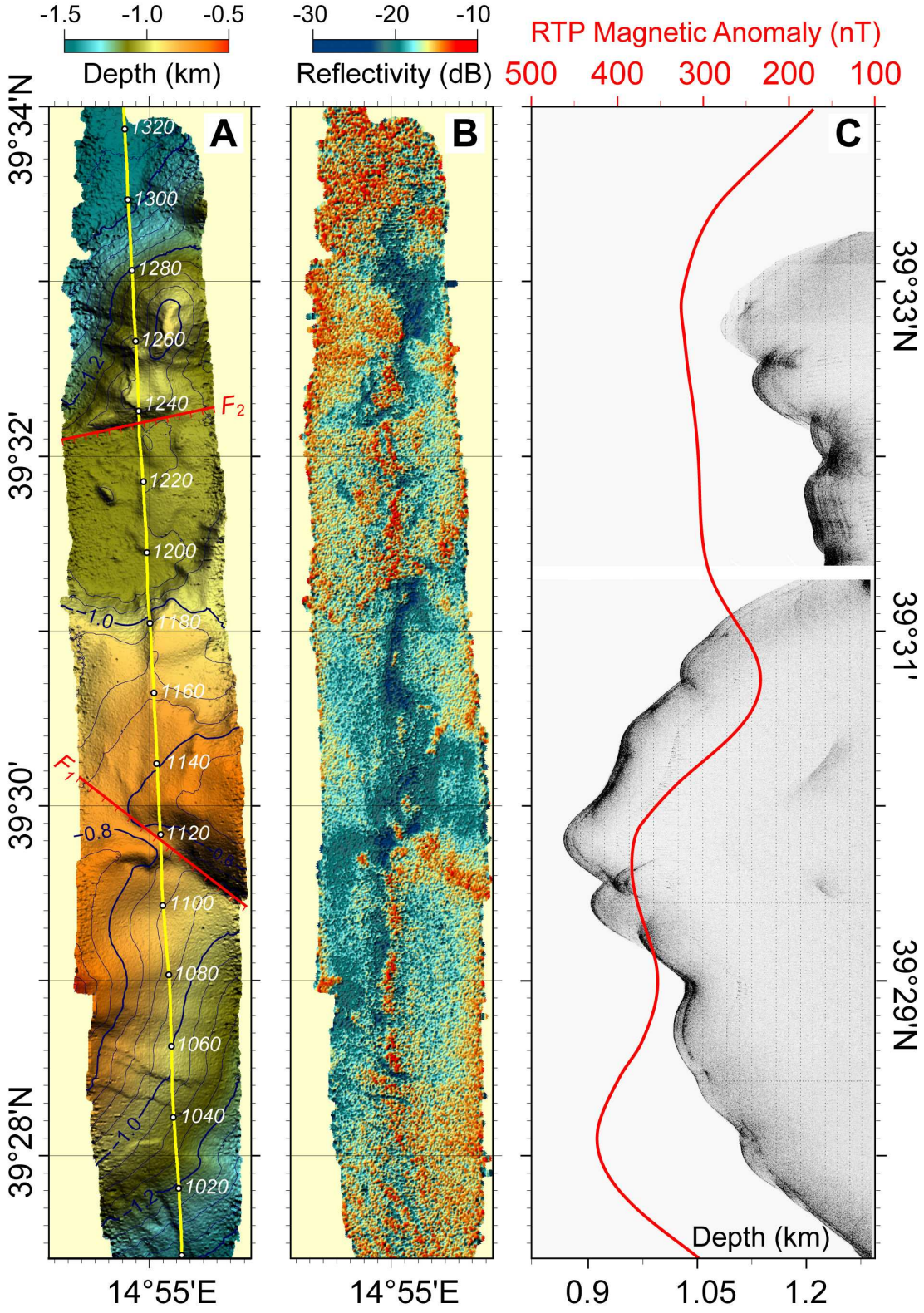

Figure 12